Rare variant in intracellular loop-2 of the ghrelin receptor reveals novel mechanisms of GPCR biased signaling and trafficking

Elsa M. Balfe [1], Alexandre Torbey [2], Lara Kohlenbach [3], Jade A. Sency [4], Asuka Inoue [5,6], Lawrence S. Barak [3], Joshua D. Gross [1,4*]

AFFILIATIONS:

[1] Departments of Nutritional Sciences and of Biobehavioral Health, The Pennsylvania State University, University Park, PA, 16802

[2] Centre Armand-Frappier Santé Biotechnologie, Institut National de la Recherche Scientifique, Laval, Canada.

[3] Department of Cell Biology, Duke University, Durham, NC 27710

[4] Huck Institute of the Life Sciences, The Pennsylvania State University, University Park, PA, 16802

[5] Graduate School of Pharmaceutical Sciences, Tohoku University, Sendai 980-8578, Japan

[6] Graduate School of Pharmaceutical Sciences, Kyoto University, Kyoto 606-8501, Japan

* To whom correspondence should be addressed: **jdg6119@psu.edu**

ABSTRACT

G protein-coupled receptors (GPCRs) are the largest class of membrane proteins and the most common pharmaceutical drug target. Through allosteric coupling, GPCRs transduce extracellular stimuli into physiologically-relevant intracellular signaling cascades via G proteins and β-arrestin (βarr). The growth hormone secretagogue receptor (GHSR) is a rhodopsin-like, peptide hormone GPCR considered a promising target for both metabolic and neurological diseases. Here, by characterizing an ultra-rare coding variant in intracellular loop-2 (ICL2) of the GHSR, $GHSR^{L149P}$ (L149P), we establish a unique role of ICL2 conformations in GPCR biased signaling, lipid modulation, and intracellular trafficking. Using an array of bioluminescence resonance energy transfer (BRET)-based assays, we show that the natural L149P mutant exhibits (i) a constitutive plasma membrane [PM] expression bias, (ii) preferential partitioning into non-lipid raft PM microdomains, (iii) enhanced agonist-directed endocytosis, and (iv) dramatic signaling bias towards βarr1/2 over $G\alpha_q$, $G\alpha_{i/o}$, and $G\alpha_{12/13}$ in a cholesterol-dependent manner. Using a combination of pharmacological and genetic tools, we demonstrate that βarr1/2 recruitment to L149P requires G protein-coupled receptor kinase-2/3 (GRK2/3)-mediated phosphorylation, but it does not utilize protein kinase C (PKC), Gβγ-dependent GRK2/3 translocation, or $G\alpha_{i/o}$, supporting a G protein-independent mechanism. Lastly, we found that βarr1/2 recruitment to L149P requires both GRK2/3 and GRK5/6, while the wild-type GHSR relies exclusively on GRK2/3, consistent with increased GRK6 pre-coupling to the L149P mutant. Collectively, our findings using a rare, natural variant reveal novel mechanisms of GPCR regulation that could be leveraged to improve personalized medicine and facilitate the rational design/discovery of $GPCR^{ICL2}$-directed drugs.

INTRODUCTION

G protein-coupled receptors (GPCRs) are the largest class of integral membrane proteins in the human genome and remain the most common pharmaceutical target [1]. As allosteric protein complexes, GPCRs convert extracellular stimuli into intracellular signaling cascades via coupling to transducers; namely, G proteins and β-arrestin (βarr) [2]. The evolutionary conservation and ubiquitous expression of GPCRs highlights how even rare, naturally-occurring GPCR mutations can precipitate clinically-relevant phenotypes [3]. To enable adaptive biological responses, GPCRs adopt a multitude of conformational states that can asymmetrically engage G proteins or βarr, thereby leading to distinct physiological outcomes in a pathway-dependent manner (*i.e.*, biased signaling). To regulate these complex processes under dynamic environmental conditions, GPCRs harbor a diverse array of allosteric binding sites accessible to various ligands, regulatory proteins, and lipids. Accordingly, GPCR biased signaling can be engendered via ligand binding (biased ligands), receptor mutations (biased receptors), differential regulatory protein or lipid expression (systems bias), and/or differential receptor or transducer subcellular distribution (location bias) [4]. Based on these principles, therapeutic interests have proliferated around the promise of 'biased' pharmaceuticals that could enhance therapeutic efficacy while simultaneously reducing side effects, toxicity, or tachyphylaxis [5].

The growth hormone secretagogue receptor (GHSR) is the cognate target of the gut-derived, peptide hormones ghrelin (endogenous agonist) and liver-expressed antimicrobial protein-2 (LEAP-2; endogenous antagonist). The GHSR is a rhodopsin-like, Class A GPCR that preferentially couples to $G\alpha_q$ and to a lesser extent, the $G\alpha_{i/o}$ and $G\alpha_{12/13}$ subfamilies [6]. Upon activation, the GHSR is phosphorylated by intracellular kinases, including $G\alpha_q$-dependent protein kinase C (PKC) and $G\beta\gamma$-dependent G protein-coupled receptor kinase 2/3 (GRK2/3), leading to βarr recruitment and subsequent desensitization, internalization/endocytosis, endosomal trafficking, and βarr-mediated signaling [7]. The GHSR is expressed both centrally and peripherally, and it serves as an integral 'rheostat' of energy balance, metabolism, reward, neuronal health, and stress/affective behavior [8]. Accordingly, the GHSR is a rational pharmaceutical drug target for several metabolic and neurological diseases [9]. The GHSR can stabilize conformations conducive to biased signaling, suggesting that the discovery of biased GHSR ligands or receptors is mechanistically feasible [6, 9-14]. While several GHSR X-ray crystallography and cryogenic electron microscopy (cryo-EM) structures have illuminated the molecular basis of ligand binding and receptor activation [15-18], the mechanisms and conformational signatures governing GHSR biased signaling and intracellular trafficking have not been elucidated fully [9].

Plasma membrane (PM) lipids are important allosteric regulators of GPCR expression/stability, ligand binding, and signaling [19]. Ligand binding and downstream G protein activation of the GHSR are dependent on cholesterol and sphingolipids [20] — key constituents of PM lipid raft microdomains [21].

Moreover, cholesterol has been resolved bound to transmembrane clefts in at least four out of seven GHSR structures [22], highlighting its importance in GHSR structure/function. While these effects are well-established, little is known about how membrane lipids affect GHSR partitioning within different subcellular compartments, and how these processes influence transducer coupling, downstream signaling, or receptor trafficking. Given that the GHSR is highly sensitive to diet-derived lipids and metabolic states impacting PM lipid composition [23], the cellular lipid microenvironment could play an important role in GHSR-related pathophysiology.

Recent studies suggest that GPCRs can be subdivided by their preference for specific GRK subtypes (*e.g.*, GRK2/3- *versus* GRK5/6-preferring), and that these intrinsic features determine receptor biased signaling [24,25,26]. For example, βarr-biased ligands (*e.g.*, TRV027 at angiotensin II type-1 receptor [26]) and intrinsically βarr-biased receptors (*e.g.*, atypical chemokine receptors [27]) preferentially utilize plasma membrane-anchored GRK5/6 for βarr recruitment, independently of Gβγ-mediated GRK2/3 translocation from the cytosol to the PM [25]. While this is logical, as βarr-biased signaling should not produce free Gβγ (*i.e.*, no G protein activation), a subset of GPCRs have been shown to recruit GRK2/3 and/or βarr in a Gβγ-independent manner [28]. Critically, to our knowledge, a systematic analysis of GRK-dependent GHSR signaling has not been performed previously.

In this study, we identify and characterize an ultra-rare, coding variant in intracellular loop-2 (ICL2) of the GHSR, Leu149Pro (L149P). The $Leu149^{ICL2}$ site (Ballesteros-Weinstein number 34.51) is +7 amino acids downstream of the highly conserved E/DRY motif, and we have shown that non-natural $GHSR^{Leu149}$ mutations regulate receptor bias and trafficking [10, 14]. Furthermore, Leu149 is situated within the short GHSR-ICL2 α-helix, which is critical for G protein activation [29]. Structural data reveal that the short ICL2 α-helix is present in five out of seven GHSR structures resolved to-date [13-16]; thus, we hypothesized that mutations in $Leu149^{ICL2}$ disrupt the α-helical structure/stability of ICL2 and thereby, exert pronounced effects on receptor expression/function.

Consistent with our prediction, we found that the natural L149P mutant exhibits a dramatic expression and signaling bias, as well as altered lipid interactions and intracellular trafficking, including: (i) a constitutive expression bias towards the PM over endosomes, (ii) reduced clustering within cholesterol-enriched lipid rafts, (iii) preferential partitioning into more disordered, non-lipid raft PM microdomains, (iv) enhanced agonist-directed endosomal translocation despite reduced endocytosis from lipid rafts, (v) dramatic signaling bias towards βarr1/2 over multiple G protein subfamilies, (vi) G protein-independent GRK2/3 and βarr1/2 recruitment, and (vii) a GRK-subtype class switch from GRK2/3-dependent receptor to a GRK2/3/5/6-dependent receptor. Collectively, our results using an ultra-rare, naturally-occurring GHSR mutant support that the conformational state of ICL2 governs GHSR biased signaling, lipid-dependent subcellular distribution, and intracellular trafficking.

RESULTS

The ultra-rare, natural variant — GHSR^{L149P} — exhibits altered subcellular distribution and trafficking in a cholesterol-dependent manner.

Our prior work shows that contiguous residues in GHSR^{ICL2} — located +6 and +7 amino acids downstream of the E/DRY motif (Pro148$^{34.50}$ and Leu149$^{34.51}$, respectively) — are important for both signaling bias and receptor trafficking [10, 14]. To determine if naturally-occurring mutations exist in either of these conserved residues, we searched publicly-available genomic databases (NCBI Database for Single Nucleotide Polymorphisms [dbSNP]; build 156, released September 21st, 2022; https://www.ncbi.nlm.nih.gov/snp/rs1390872592) and identified Leu149>Pro (rs1390872592; **Figure 1a**), an ultra-rare nonsynonymous coding variant (reported allele frequency = 1/250,994). We did not identify any natural variants in the upstream Pro148$^{34.50}$ site, perhaps due to its high conservation across rhodopsin-like GPCRs [30]; thus, we proceeded with characterization of only the L149P mutant.

Our previous work demonstrated that non-natural GHSR mutations in the Pro148-Leu149^{ICL2} motif affects plasma membrane (PM) expression [10]; thus, we first tested the basal cell surface expression and agonist-induced internalization of the L149P mutant upon transient expression in HEK293/T cells using on-cell enzyme-linked immunosorbent assay (ELISA). Consistent with previously characterized GHSR-Leu149^{ICL2} mutants [10, 14], the basal surface expression of L149P was increased by >2-fold relative to the wild-type GHSR (WT) (**Figure 1b**). Both the WT and L149P receptors underwent agonist-induced internalization following stimulation with human acyl-ghrelin (ghrelin) or the synthetic unbiased agonist MK0677 (**Figure 1b**); however, ghrelin-stimulated WT receptor internalization did not reach statistical significance (p=0.06). The magnitude of ghrelin- and MK0677-induced L149P internalization was ~2-fold greater than the WT receptor (66% versus 32.5%, respectively) (**Figure 1b**), supporting that the L149P mutant undergoes enhanced agonist-directed endocytosis.

To determine if increased basal L149P surface expression was due to altered constitutive, dynamin-dependent internalization (*i.e.*, 'receptor cycling'), we also co-expressed a dominant negative dynamin mutant (Dyn^{K44A}) in the same experiments. Dynamin inhibition markedly increased the basal surface expression of both the WT and L149P receptors, albeit to a greater extent for the WT receptor (250% increase relative to WT-pcDNA) compared to L149P (129% increase relative to L149P-pcDNA) (**Figure 1b**). Notably, basal WT surface expression co-expressed with Dyn^{K44A} was remarkably similar to L149P at baseline, supporting that reduced constitutive internalization/cycling of the L149P mutant may account for its enhanced surface expression. The co-expression of Dyn^{K44A} completely blocked ghrelin and MK0677-induced internalization of WT and L149P, indicating that both receptors undergo dynamin-dependent endocytosis upon agonist stimulation.

To determine total receptor expression, we performed in-cell ELISA assays upon transient expression of L149P at an equal (100ng) or surface expression-adjusted (50ng) mass relative to the WT receptor (100ng). Expression of L149P at a 1:2 ratio produced similar total receptor expression; whereas, a 1:1 ratio of L149P-to-WT produced >2-fold the total expression of L149P relative to the WT receptor (**Figure 1c**), similar to its increased surface expression (see **Figure 1b**). Thus, in all subsequent experiments, we transfected an expression-adjusted ratio of L149P-to-WT receptor (1:2).

We next evaluated PM partitioning and endosomal trafficking of the natural L149P mutant using a bystander bioluminescence energy resonance transfer (bBRET)-based approach; including, the mVenus-tagged (i) non-lipid raft-targeting PM sensor CAAX [prenylation CAAX box of KRas], (ii) the lipid raft-targeting PM sensor myristoyl-palmitoylated (MyrPalm), and (iii) the early endosome-targeting sensor 2xFYVE [zinc finger domain of endofin], which binds phosphatidylinositol 3-phosphate [PIP_3] (**Figure 1d**). Relative to WT, the L149P mutant had increased PM localization within both non-raft (CAAX) and lipid raft (MyrPalm) microdomains at baseline (**Figure 1e**); however, lipid raft enrichment (MyrPalm:CAAX ratio) of L149P was reduced relative to WT (**Figure 1f**), supporting that the L149P mutant preferentially partitions into non-raft PM microdomains. To confirm these effects, we pretreated cells with methyl-β-cyclodextrin (MβCD), a membrane cholesterol chelator, then re-evaluated PM microdomain partitioning. MβCD pretreatment reversed the reduction in L149P lipid raft enrichment, such that, the L149P mutant exhibited increased partitioning into lipid rafts following cholesterol depletion (**Figure 1g**).

Additionally, basal L149P localization in early endosomes (2xFYVE) was markedly reduced relative to the WT receptor (**Figure 1h**). By comparing the ratio of non-raft PM (CAAX) and lipid raft PM (MyrPalm) to endosomal (2xFYVE) localization, the results further supported that the L149P mutant displays a constitutive PM expression bias relative to endosomes (**Figure 1i**), consistent with enhanced constitutive surface expression and reduced receptor recycling measured by ELISA (see **Figure 1b-c**). Furthermore, MβCD pretreatment completely reversed the PM expression bias of L149P, supporting the differential subcellular distribution of the L149P mutant is cholesterol-dependent (**Figure 1j**).

To test agonist-induced endocytosis between each subcellular compartment, we stimulated bBRET sensor-expressing cells with a saturating concentration of ghrelin (1μM) and measured the change in CAAX, MyrPalm, and 2xFYVE localization with the WT or L149P receptors over two-hours. Both WT and L149P displayed minimal endocytosis from non-raft (CAAX) microdomains, and their magnitudes did not differ (**Figure 1k**). In contrast, agonist-induced WT receptor endocytosis from lipid rafts (MyrPalm) was robust, while lipid raft-mediated L149P endocytosis was substantially decreased relative to WT (**Figure 1l**). Conversely, both the rate and magnitude of ghrelin-induced L149P endosomal translocation was markedly increased relative to WT (**Figure 1m**), consistent with increased agonist-induced internalization measured by ELISA (see **Figure 1b**). Upon cholesterol depletion with MβCD, ghrelin-induced WT receptor endocytosis from lipid rafts was reduced, while L149P endocytosis was unaffected (**Figure 1n**),

consistent with the reduced L149P clustering in lipid rafts (see **Figure 1f**). Notably, WT receptor endocytosis from lipid rafts was reduced to a level similar to the L149P mutant under cholesterol-replete (vehicle-treated) conditions (**Figure 1n**), suggesting that the reduction in lipid raft-mediated L149P endocytosis (see **Figure 1l**) is related to membrane cholesterol levels. Furthermore, ghrelin-induced endosomal translocation of the L149P mutant, but not WT, was significantly reduced upon MβCD pretreatment (**Figure 1o**), suggesting that increased agonist-directed L149P endosomal translocation (see **Figure 1m**) is, at least partially, cholesterol-dependent.

Collectively, the results in **Figure 1** support that the L149P mutant exhibits a cholesterol-dependent (i) PM expression bias relative to endosomes due to attenuated constitutive internalization/cycling, (ii) reduction in lipid raft clustering and preferential partitioning into non-raft PM microdomains, (iii) reduction in lipid raft-mediated, agonist-directed endocytosis, and (iv) enhancement in agonist-directed internalization and endosomal translocation. For all descriptive statistics (mean ± SEM) and statistical analyses in **Figure 1**, see **Supplementary Table 1**.

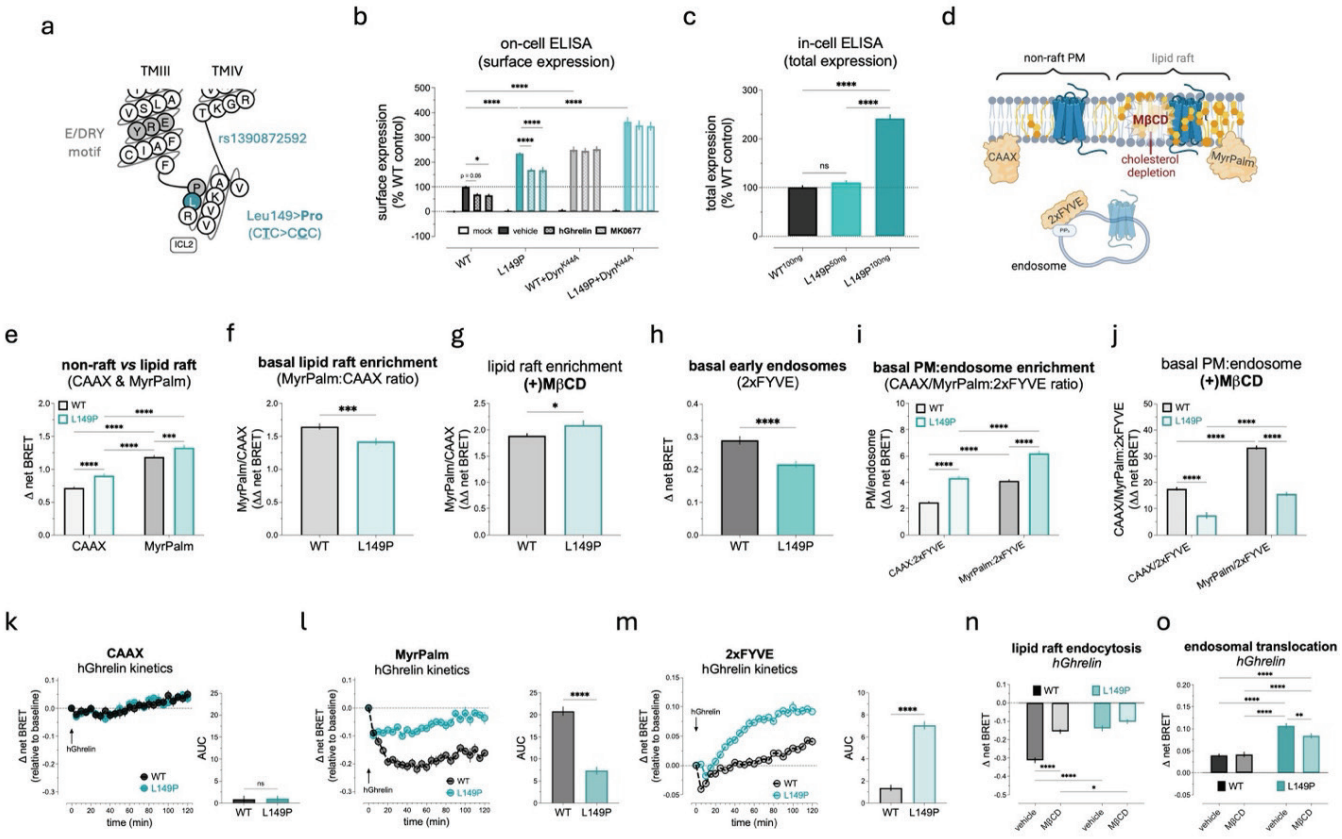

Figure 1. Subcellular distribution, PM partitioning, and trafficking of the natural L149P mutant. (a) GHSR Snake plot; E/DRY motif in TMIII (grey), Pro148^{ICL2} (grey), and Leu149^{ICL2} (teal). Non-synonymous SNP in Leu149 codon (CTC>CCC) resulting in the L149P missense mutation. **(b)** Basal and agonist (1μM)-stimulated (45-minutes, 37°C) surface expression (on-cell ELISA) in cells transiently expressing GHSR-WT^{100ng} (black/grey) or L149P^{100ng} (teal) ± Dyn^{K44A}, analyzed by two-way ANOVA and Holm-Sidak's post-hoc test. **(c)** Total receptor expression (in-cell ELISA) in cells transiently expressing WT^{100ng}

(black), L149P^{50ng} (light teal), or L149P^{100ng} (dark teal), analyzed by one-way ANOVA. **(d)** bBRET sensors; mVenus-tagged CAAX (non-raft PM), MyrPalm (lipid raft PM), and 2xFYVE (early endosomes). MβCD (red) was used to deplete PM cholesterol. **(e)** Basal non-raft (CAAX) and lipid raft (MyrPalm) localization with WT^{RLuc8} (grey) or L149P^{RLuc8} (teal), analyzed by two-way ANOVA and Tukey's post-hoc test. **(f)** Basal lipid raft enrichment calculated using the ratio of MyrPalm:CAAX (ΔΔ net BRET), derived from *Panel e*, then analyzed by *t*-test. **(g)** Basal lipid raft enrichment following MβCD pretreatment (3mM, 30-minutes, 37°C), analyzed by *t*-test. **(h)** Basal early endosomal (2xFYVE) localization, analyzed by *t*-test. **(i)** Basal PM enrichment over endosomes, derived from *Panels e* (CAAX and MyrPalm) and *Panel h* (2xFYVE), calculated using the ratio of CAAX:2xFYVE or MyrPalm:2xFYVE (ΔΔ net BRET), then analyzed by two-way ANOVA and Tukey's post-hoc test. **(j)** Basal PM enrichment over endosomes following MβCD pretreatment, then analyzed by two-way ANOVA and Tukey's post-hoc test. Kinetics (*left*) and area under the curve (AUC; *right*) of hGhrelin (1μM)-induced **(k)** CAAX, **(l)** MyrPalm, and **(m)** 2xFYVE localization with WT^{RLuc8} (black) or L149P^{RLuc8} (teal); AUC was evaluated statistically by *t*-test. hGhrelin (1μM)-induced **(n)** endocytosis from lipid rafts (MyrPalm) and **(o)** endosomal translocation (2xFYVE) over two-hours following 30-mintute pretreatment with vehicle or MβCD, assessed by two-way ANOVA and Tukey's post-hoc test. All data are expressed as the mean ± SEM from ≥3 independent experiments in triplicate or quadruplicate.

Basal and agonist-stimulated βarr1/2 recruitment to the L149P mutant is dynamin- and cholesterol-dependent.

Non-natural missense mutations in GHSR-Leu149^{ICL2} produce βarr-bias [10, 14]; thus, we next evaluated human βarr1/2 (hβarr1/2) recruitment to the natural L149P mutant using a BRET-based approach. Basal βarr1 recruitment (**Figure 2a**) to L149P was similar to the WT receptor (**Figure 2b**). A concentration-response (C/R) analysis of ghrelin-induced βarr1 recruitment revealed that ghrelin potency (EC_{50}) at L149P was comparable to WT, while maximal efficacy (E_{max}) was reduced by 53% (**Figure 2c**). Kinetic analyses showed that a saturating concentration of ghrelin (1μM) stimulated βarr1 recruitment to L149P at a rate (K_m) similar to the WT receptor (**Figure 2d**). Similar to ghrelin, MK0677 stimulated βarr1 recruitment to L149P with equal potency and reduced efficacy (57%) relative to WT (**Figure 2e**), as well as similar βarr1 association kinetics (**Figure 2f**). A statistical evaluation of ghrelin and MK0677 E_{max} showed that βarr1 recruitment efficacy at the L149P mutant was reduced to similar extents for both agonists relative to their respective WT controls (**Figure 2g**).

Next, we tested basal and agonist-stimulated βarr2 (**Figure 2h**) recruitment to the L149P and WT receptors using a similar BRET-based approach. In contrast to βarr1, basal βarr2 recruitment to the L149P mutant was reduced relative to the WT receptor (**Figure 2i**); whereas, ghrelin-induced βarr2 recruitment to L149P was equipotent to WT and efficacy was reduced (**Figure 2j**). Notably, the magnitude of ghrelin efficacy reduction for L149P-βarr2 (34%) was less than L149P-βarr1 (53%; see **Figure 2c**), indicating that the L149P mutant recruits βarr2 more effectively than βarr1, like the WT-GHSR [14]. Furthermore, ghrelin-stimulated βarr2 association rate was similar between the L149P and WT receptors (**Figure 2i**). MK0677 potency for βarr2 recruitment at L149P was reduced mildly relative to the WT

receptor, while MK0677 efficacy was reduced by only 24% at L149P (**Figure 2l**). Like ghrelin, MK0677 elicited similar βarr2 recruitment association rate kinetics to both the WT and L149P receptors (**Figure 2m**). An analysis of ghrelin- and MK0677-βarr2 E_{max} showed that the L149P mutant had reduced agonist efficacy relative to the WT receptor (**Figure 2n**), albeit to a lesser extent than the reductions observed for βarr1 (see **Figures 2e, 2g**); moreover, MK0677-stimulated βarr2 recruitment efficacy to L149P was moderately increased relative to ghrelin efficacy (**Figure 2n**).

Recent work shows that the agonist-directed endocytosis kinetics of $G\alpha_q$-coupled GPCRs are predictive of βarr efficacy [31]. Considering increased L149P surface expression and endosomal translocation (see **Figure 1**), we next assessed whether these characteristics were associated with L149P-βarr efficacy (see **Figures 2c-d, 2g** and **2j-k, 2n**). To test this, we co-expressed Dyn^{K44A} (**Figure 2o**) and assessed βarr1/2 recruitment. Because MK0677 displayed a similar βarr1/2 recruitment profile to ghrelin, only ghrelin was tested in these mechanistic experiments. Dyn^{K44A} co-expression did not affect basal βarr1 recruitment to the L149P or WT receptors (**Figure 2p**); whereas, Dyn^{K44A} markedly reduced ghrelin-stimulated βarr1 recruitment efficacy, but not potency, at both receptors (**Figure 2q-r**). Furthermore, Dyn^{K44A} co-expression significantly decreased ghrelin-βarr1 efficacy at the WT receptor to a level nearly identical to L149P in the absence of Dyn^{K44A} (**Figure 2q-r**).

For βarr2, basal recruitment to L149P was unaffected by Dyn^{K44A} co-expression, while basal βarr2 recruitment to the WT receptor was reduced to a level nearly identical to L149P in the absence of Dyn^{K44A} (**Figure 2s**). Additionally, ghrelin-stimulated βarr2 recruitment was reduced upon Dyn^{K44A} co-expression for both the L149P and WT receptors, and the reduction observed for the WT produced a nearly identical E_{max} compared to L149P in the absence of Dyn^{K44A} (**Figures 2t-u**). These results together support that reduced basal βarr2 recruitment (see **Figure 2i**) and reduced agonist βarr1/2 efficacy (see **Figures 2c,g and 2j,n**) at the L149P mutant are likely due to its PM expression bias and/or distinct endosomal trafficking profile (see **Figure 1**). Furthermore, our findings support that the constitutive WT-GHSR endocytosis is required for basal βarr2, but not βarr1 recruitment; whereas, constitutive WT-GHSR endocytosis is required for the agonist-directed recruitment of both βarr1 and βarr2.

To test the effect of membrane cholesterol on βarr, we next depleted cholesterol with MβCD (**Figure 2v**), then assessed basal and ghrelin-stimulated βarr1/2 recruitment to the L149P and WT receptors. MβCD pretreatment did not appreciably affect basal βarr1 recruitment to WT or L149P compared to their respective vehicle controls; however, there was a mild reduction in basal βarr1 recruitment to the MβCD-pretreated L149P relative to the vehicle-pretreated WT receptor (**Figure 2w**). Ghrelin-stimulated βarr1 recruitment potency was moderately decreased at L149P (2.6-fold) and WT (1.8-fold) receptors (**Figure 2x**). Furthermore, ghrelin E_{max} at L149P was significantly reduced by MβCD pretreatment, while the trend for reduced ghrelin E_{max} at the WT receptor did not reach statistical significance (**Figure 2y**).

In contrast to βarr1, MβCD pretreatment decreased basal βarr2 recruitment to the WT receptor but did not affect L149P (**Figure 2z**), suggesting that reduced L149P-βarr2 recruitment at baseline is cholesterol-dependent. Additionally, MβCD pretreatment attenuated ghrelin-induced βarr2 recruitment potency (**Figure 2aa**) and efficacy (**Figures 2aa-bb**) at both L149P and WT, although the effects were larger for the L149P mutant (**Figures 2aa-bb**) and identical in magnitude to βarr1 (see **Figures 2x-y**). Notably, MβCD pretreatment reduced ghrelin E_{max} at the WT receptor to a level statistically similar to the vehicle-pretreated L149P, supporting that the moderate reduction in βarr2 recruitment efficacy to L149P at baseline (~35%) is cholesterol-dependent. Together, these results support that (i) membrane cholesterol, at least partially, explains the selective reduction in basal βarr2 recruitment to the L149P mutant relative to βarr1 and (ii) agonist-stimulated βarr1/2 recruitment to both the L149P and WT receptors is cholesterol-dependent, albeit more important for L149P.

Collectively, the results in **Figure 2** demonstrate that the L149P mutant recruits βarr1/2 with high agonist potency, moderately reduced efficacy, and normal association rate kinetics relative to the WT-GHSR. Additionally, L149P exhibits a selective reduction in basal βarr2 recruitment and higher agonist efficacy for βarr2 relative to βarr1, perhaps due to the lower baseline. Furthermore, our results suggest that the βarr1/2 recruitment characteristics of L149P are, at least partially, related to its PM expression bias, differential PM microdomain partitioning, and/or differential endosomal trafficking (see **Figure 1**). For all descriptive data, C/R analyses, and statistics in **Figure 2**, see **Supplementary Table 2**.

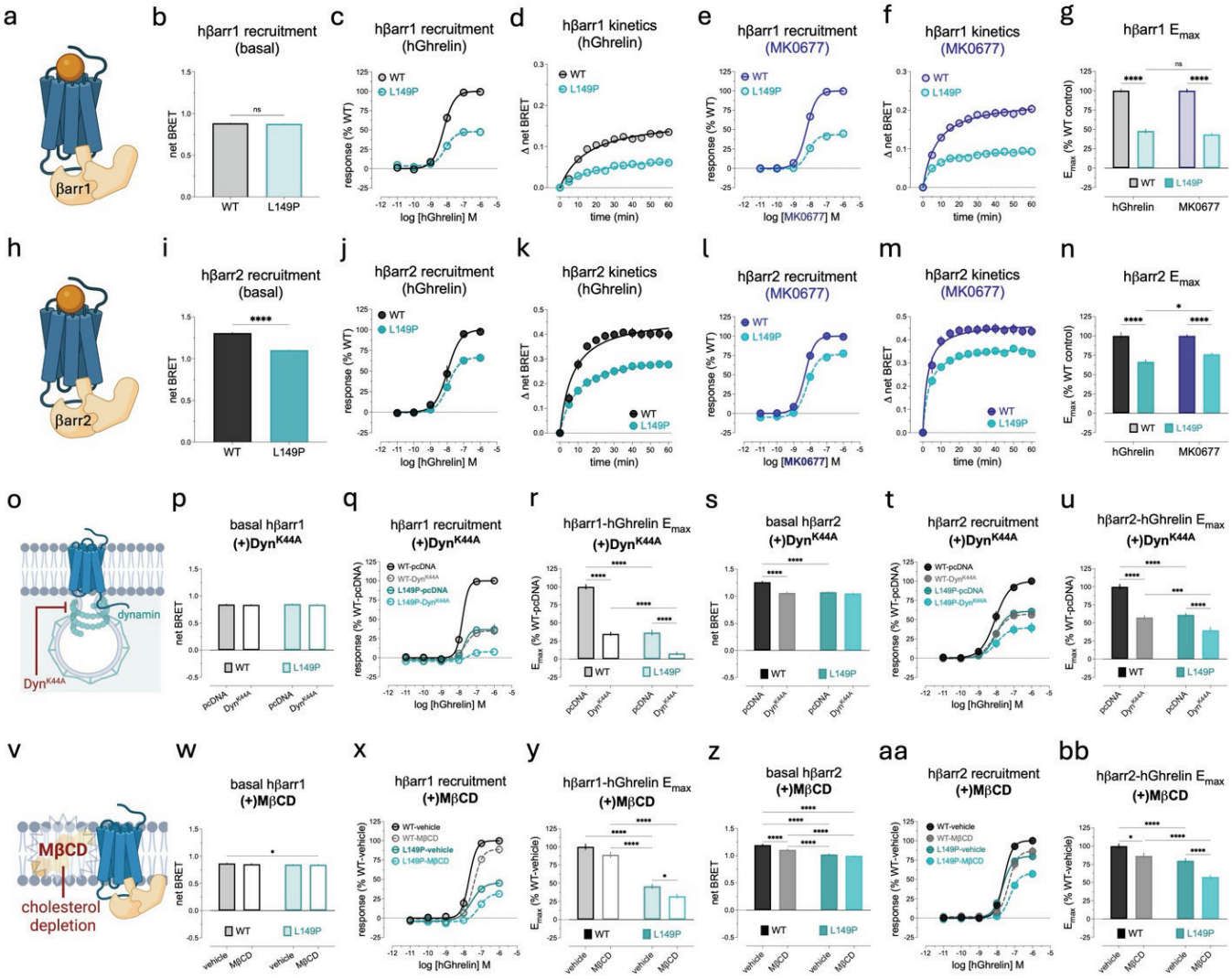

Figure 2. Basal and agonist-stimulated βarr1/2 recruitment to L149P is partially dynamin- and cholesterol-dependent. **(a)** βarr1 (light orange) coupling to GHSR (blue). **(b)** Basal hβarr1 recruitment to WT (grey) and L149P (light teal) expressed as absolute net BRET. **(c)** hGhrelin (C/R)-induced hβarr1 recruitment. **(d)** hGhrelin (1μM)-induced hβarr1 recruitment kinetics, derived from *Panel c*. **(e)** MK0677 (C/R)-induced hβarr1 recruitment to WT (light blue) and L149P (light teal). **(f)** MK0677 (1μM)-induced hβarr1 recruitment kinetics, derived from *Panel e*. **(g)** hGhrelin (*left*) and MK0677 (*right*) E_{max} for hβarr1 recruitment, derived from data in *Panel c* and *Panel e*, respectively. **(h)** βarr2 (light orange) coupling to GHSR (blue). **(i)** Basal hβarr2 recruitment to WT (black) and L149P (dark teal). **(j)** hGhrelin (C/R)-induced hβarr2 recruitment. **(k)** hGhrelin (1μM)-induced hβarr2 recruitment kinetics, derived from *Panel j*. **(l)** MK0677 (C/R)-induced hβarr2 recruitment to WT (dark blue) and L149P (dark teal). **(m)** MK0677 (1μM)-induced hβarr2 recruitment kinetics, derived from *Panel l*. **(n)** hGhrelin (*left*) and MK0677 (*right*) E_{max} for hβarr2, derived from data in *Panel j* and *Panel l*, respectively. Basal activity was evaluated by a *t*-test. All kinetic data represent the maximal response at each time point (Δ net BRET relative to baseline) and were fit by Michalis-Menton non-linear regression to derive K_m and V_{max}. All E_{max} data were normalized to the WT-E_{max} for each respective agonist (set at 100%), then analyzed by two-way ANOVA followed by Tukey's post-hoc test. **(o)** Dyn^{K44A} inhibiting receptor endocytosis. **(p)** Basal, **(q)** hGhrelin (C/R)-induced, **(r)** hGhrelin E_{max} for hβarr1 (derived from *Panel q*) to WT (grey) or L149P (light teal) co-expressing pcDNA or Dyn^{K44A}. **(s)** Basal, **(t)** hGhrelin (C/R)-induced, and **(u)** hGhrelin E_{max} for hβarr2 (derived from *Panel t*)

to WT (black/dark grey) or L149P (dark teal) co-expressing pcDNA or Dyn^{K44A}. **(v)** MβCD-mediated depletion of membrane cholesterol (red) and βarr (light orange) recruitment to GHSR (blue). **(w)** Basal, **(x)** hGhrelin (C/R)-induced, and **(y)** hGhrelin E_{max} for hβarr1 (derived from *Panel* x) to WT (grey) or L149P (light teal) pretreated with 3mM MβCD (30-minutes, RT) or vehicle. **(a)** Basal, **(aa)** hGhrelin-induced, and **(bb)** hGhrelin E_{max} for hβarr2 (derived from *Panel aa*) to WT (black) or L149P (dark teal) pretreated with MβCD or vehicle. All basal and E_{max} data between *Panels p-bb* were analyzed by two-way ANOVA followed by Tukey's post-hoc test. All data represent the pooled mean ± SEM from ≥3 independent experiments in triplicate.

L149P-mediated inhibition of G protein signaling is Gα subtype-specific and cholesterol-independent.

Next, we tested if the L149P mutant could couple to and/or activate $G\alpha_q$ — the preferential G protein for the GHSR [6]. First, we employed the BRET-based TRUPATH assay to evaluate $G\alpha_q$ activation, which measures $G\alpha_q$-Gβγ dissociation upon guanine nucleotide exchange (GDP>GTP) [32] (**Figure 3a**). The GHSR exhibits remarkably high constitutive $G\alpha_q$ activity (≥50% ghrelin E_{max} [33]); thus, to provide a more direct measure, we included an additional pcDNA empty vector (EV) condition to normalize our basal data (*i.e.*, derive Δ net BRET relative to EV/background). Constitutive $G\alpha_q$ dissociation was reduced by >70% in the L149P mutant relative to WT receptor (**Figure 3b**). Furthermore, ghrelin- (**Figure 3c**) and MK0677- (**Figure 3d**) stimulated $G\alpha_q$ dissociation was abolished at L149P, supporting that the L149P mutant confers complete βarr-bias (see **Figure 2**) relative to $G\alpha_q$. An analysis of agonist E_{max} showed that both ghrelin and MK0677 agonism is completely abolished at L149P (E_{max} = 0; **Figure 3e**), suggesting that the L149P mutation reduces $G\alpha_q$ activation by preferentially stabilizing an inactive conformation of the agonist-bound GHSR.

Subsequently, we tested if the L149P mutant could still couple to $G\alpha_q$, despite its inability to activate the $G\alpha_q$ heterotrimer (*i.e.*, initiate guanine nucleotide exchange). To test this, we employed the BRET-based mini-G_q sensor (**Figure 3f**), which mimics the nucleotide-free, G protein active state and removes the Gα's membrane anchoring, Gβγ binding, and α-helical domain [34]. Constitutive mini-G_q recruitment was nearly abolished at the L149P mutant (**Figure 3g**); but to our surprise, ghrelin (**Figure 3h**) and MK0677 (**Figure 3i**) potency for mini-G_q recruitment was similar to WT, and efficacy was reduced by ~75%, but not abolished (**Figure 3j**). Taken together with our TRUPATH results (see **Figures 3c-e**), these findings suggest that the L149P mutation selectively disrupts agonist-induced guanine nucleotide exchange, consistent with other ICL2 perturbations [35,36].

The GHSR preferentially couples to $G\alpha_q$, but it also couples to G proteins within the $G\alpha_{i/o}$ and $G\alpha_{12/13}$ families — especially, $G\alpha_{i2}$, $G\alpha_{oA}$, and $G\alpha_{13}$ — albeit with lower intrinsic efficacy [6]. We next tested (i) if the L149P mutant could activate these G proteins and (ii) if membrane cholesterol differentially affected signaling across G protein subfamilies. Using $G\alpha_q$ as a control (**Figure 3k**), we confirmed both minimal L149P constitutive activity (**Figure 3l**) and no agonist-induced $G\alpha_q$ activation (**Figures 3m-n**) at baseline.

Following MβCD pretreatment, there was a mild, but statistically significant reduction in ghrelin potency for WT-mediated $G\alpha_q$ activation (**Figure 3m**) and no change in efficacy (**Figures 3l-n**). To our surprise, $G\alpha_{13}$ (**Figure 3o**) constitutive activity was comparable between the vehicle-pretreated WT and L149P receptors; whereas, MβCD significantly increased WT constuitive activity and did not affect L149P (**Figure 3p**). In contrast, ghrelin-stimulated $G\alpha_{13}$ activation was abolished at L149P, while ghrelin efficacy was reduced at the WT receptor (**Figures 3q-r**). For $G\alpha_{i2}$ (**Figure 3s**), both constitutive (**Figure 3t**) and ghrelin-stimulated activation (**Figures 3u-v**) were markedly reduced at L149P, but not abolished, in a cholesterol-independent manner for both receptors (**Figures 3t-v**). For $G\alpha_{oA}$ (**Figure 3w**), constitutive (**Figure 3x**) and ghrelin-stimulated activation (**Figure 3y-z**) were markedly reduced, but not abolished, at L149P upon vehicle pretreatment; whereas, MβCD pretreatment decreased agonist potency and efficacy only at the WT receptor (**Figure 3y-z**). In summary, these results support four key findings: The L149P mutant displays (i) nearly abolished $G\alpha_q$ signaling, likely due to disrupted guanine nucleotide exchange; (ii) no agonist-stimulated $G\alpha_q$ or $G\alpha_{13}$ activation and $G\alpha_{i/o}$ partial agonism; (iii) normal $G\alpha_{13}$ constitutive activity despite markedly reduced $G\alpha_q$ and $G\alpha_{i/o}$ constitutive activity; (iv) cholesterol-independent effects on G proteins, while the WT-GHSR requires membrane cholesterol for most G protein signaling. For all descriptive data, C/R curve analyses, and statistics in **Figure 3**, see **Supplementary Table 4.**

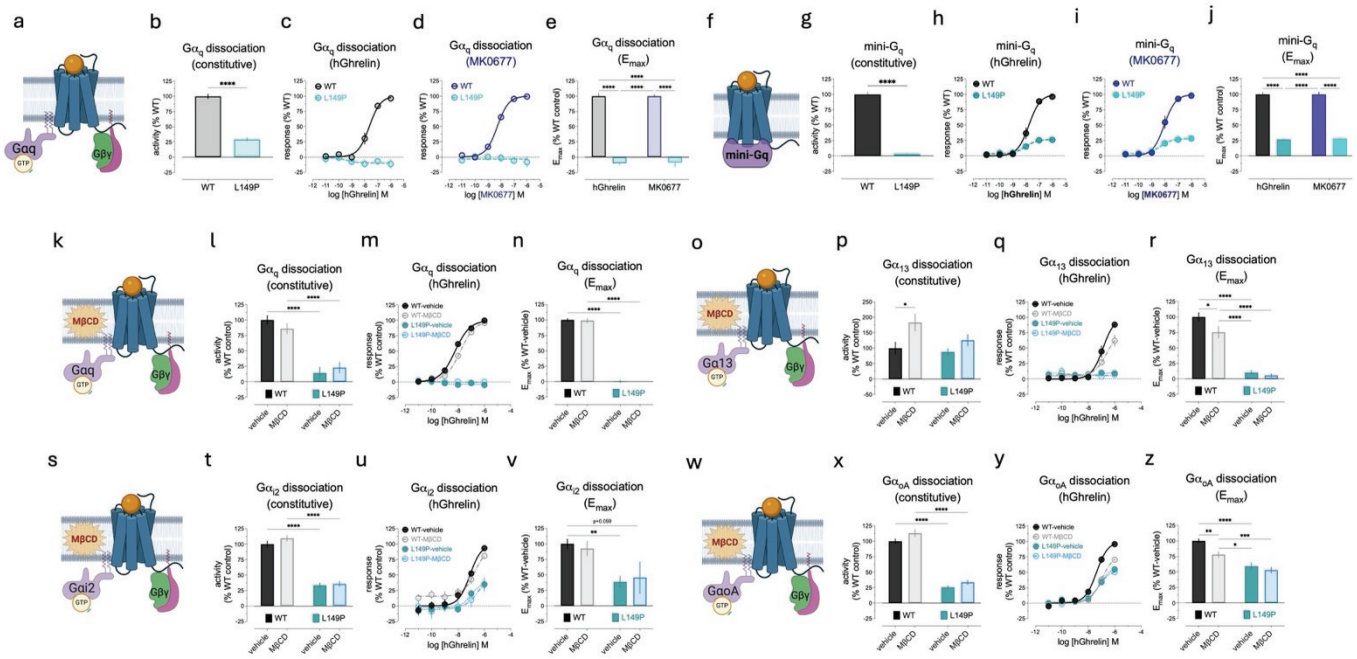

Figure 3. G protein signaling profile at the L149P mutant. (a) $G\alpha_q$ dissociation into $G\alpha_q$-GTP and free $G\beta\gamma$, measured by TRUPATH. **(b)** Constitutive $G\alpha_q$ activity of WT (grey) and L149P (light teal). **(c)** hGhrelin (C/R)-stimulated $G\alpha_q$ dissociation at WT and L149P. **(d)** MK0677 (C/R)-stimulated $G\alpha_q$ dissociation at WT (light blue) and L149P. **(e)** hGhrelin (*left*) and MK0677 (*right*) E_{max} for $G\alpha_q$ dissociation, derived from data in *Panels c-d*. **(f)** mini-G_q coupling to GHSR (blue). **(g)** Constitutive mini-G_q recruitment of WT (black) and L149P (dark teal). **(h)** hGhrelin (C/R)-stimulated mini-G_q recruitment to WT and L149P. **(i)**

MK0677 (C/R)-stimulated mini-G_q recruitment to WT (dark blue) and L149P. **(j)** hGhrelin (*left*) and MK0677 (*right*) E_{max} for mini-G_q recruitment, derived from data in *Panels h-i*. **(k)** $G\alpha_q$ dissociation ± MβCD. **(l)** Constitutive, **(m)** hGhrelin (C/R), and **(n)** hGhrelin E_{max} for $G\alpha_q$ at WT-vehicle (black), L149P-vehicle (dark teal), WT-MβCD (grey), and L149P-MβCD (light blue). **(o)** $G\alpha_{13}$ dissociation ± MβCD. **(p)** Constitutive, **(q)** hGhrelin (C/R), and **(r)** hGhrelin E_{max} for $G\alpha_{13}$. **(s)** $G\alpha_{i2}$ dissociation ± MβCD. **(t)** Constitutive, **(u)** hGhrelin (C/R), and **(v)** hGhrelin E_{max} for $G\alpha_{i2}$. **(w)** $G\alpha_{oA}$ dissociation ± MβCD. **(x)** Constitutive, **(y)** hGhrelin (C/R), and **(z)** hGhrelin E_{max} for $G\alpha_{oA}$. Constitutive activity was calculated by subtracting the absolute net BRET of EV/pcDNA plus biosensor (0%) from the absolute net BRET of receptor-alone to derive Δ net BRET, then normalizing to WT (100%). Constitutive activity was evaluated by a *t*-test (*Panels b* and *g*) or two-way ANOVA (*Panels l*, *p, t*, and *x*) followed by Tukey's post-hoc test. E_{max} data were analyzed by two-way ANOVA followed by Tukey's post-hoc test. All data represent the pooled mean ± SEM from ≥3 independent experiments run in duplicate or triplicate.

βarr recruitment to the L149P mutant requires GRK2/3-mediated phosphorylation but does not require G protein-dependent PKC or GRK2/3 activation.

GHSR phosphorylation following $G\alpha_q^{GTP}$-dependent PKC activation and free Gβγ-dependent GRK2/3 translocation [37] are required for βarr recruitment, with the latter mediated by Gβγ interaction with the pleckstrin homology (PH) domain of GRK2/3 [38]. Accordingly, we next tested how the L149P mutant could elicit βarr-bias despite minimal G protein signaling (see **Figure 3**).

First, we used a pharmacological approach by employing a pan-PKC inhibitor, Go6983, or the selective GRK2/3 inhibitor, Compound 101 (Cmp101). To both test constitutive βarr recruitment and also control for potential confounding effects of inhibitors (*e.g.*, Go6983 coloration), we included an EV/pcDNA control, as performed in G protein assays (see **Figure 3**). For βarr1 (**Figure 4a**), Go6983-alone and Cmp101-alone did not affect constitutive βarr1 recruitment to the WT receptor, while the combined pretreatment of Go6983 plus Cmp101 reduced constitutive βarr1 recruitment compared to Cmp101-alone, but not vehicle (**Figure 4b**). In contrast, Go6983-alone moderately, and Cmp101-alone markedly, reduced ghrelin-stimulated βarr1 recruitment efficacy to the WT receptor (29% *versus* 83% decrease, respectively), while ghrelin potency was not affected (**Figures 4c-d**). Go6983 plus Cmp101 had an additive effect, which nearly abolished βarr1 recruitment efficacy to the WT receptor (**Figures 4c-d**). At L149P, constitutive βarr1 recruitment was not affected by Go6983-alone, Cmp101-alone, or Go6983 plus Cmp101 (**Figure 4e**). In contrast to WT, Go6983-alone did not affect ghrelin-stimulated βarr1 recruitment efficacy at L149P; whereas, Cmp101-alone and Go6983 plus Cmp101 reduced βarr1 recruitment efficacy to similar degrees (**Figure 4f-g**), and ghrelin potency was not affected (**Figure 4f**).

For βarr2 (**Figure 4h**), similar effects were observed for both constitutive (**Figures 4i, 4l**) and agonist-stimulated βarr2 recruitment at the WT (**Figures 4j-k**) and L149P (**Figure 4m-n**) receptors, but with two exceptions: First, constitutive L149P-βarr2 recruitment trended towards an increase following Cmp101-alone relative to vehicle, but statistical significance emerged only when compared to Go6983 plus

Cmp101 (**Figure 4l**). Second, Go6983 plus Cmp101 decreased ghrelin-stimulated L149P-βarr2 recruitment relative to Cmp101-alone, supporting a potential additive effect. While unexpected, we speculate that this might reflect background PKC activity or signaling 'crosstalk' independent of L149P-mediated signaling. Overall, the results in **Figures 4a-n** support that the WT-GHSR requires both PKC and GRK2/3 for βarr1/2 recruitment, while L149P requires only GRK2/3.

To determine if GRK2/3-dependent βarr1 recruitment to the L149P mutant requires GRK2/3-mediated phosphorylation and/or Gβγ-dependent GRK2/3 translocation, we next co-expressed the phosphorylation-deficient GRK2 mutant, $GRK2^{K220R}$, or pretreated cells with the Gβγ-GRK2/3 interfering peptide, GRK2i, then first tested βarr1 recruitment (**Figure 4o**). Constitutive βarr1 recruitment to the receptor was not affected by $GRK2^{K220R}$ or GRK2i relative to control (pcDNA-vehicle). However, GRK2i mildly increased constitutive WT-βarr1 recruitment relative to $GRK2^{K220R}$ (**Figure 4p**). Ghrelin-stimulated WT-βarr1 recruitment efficacy was markedly reduced by $GRK2^{K220R}$ (82% decrease), and GRK2i led to a moderate reduction in efficacy (19% decrease) (**Figure 4q-r**). Neither $GRK2^{K220R}$ nor GRK2i affected ghrelin potency at the WT receptor (**Figure 4q**). For the L149P mutant, GRK2i increased constitutive βarr1 recruitment relative to control (**Figure 4s**), but the effect was small. Importantly, while $GRK2^{K220R}$ markedly reduced βarr1 recruitment efficacy to the L149P mutant, GRK2i had no effect (**Figure 4t-u**). Ghrelin potency for L149P-βarr1 recruitment was not affected by $GRK2^{K220R}$ or GRK2i (**Figure 4t-u**).

In parallel βarr2 experiments (**Figure 4v**), $GRK2^{K220R}$ abolished WT constitutive activity, while GRK2i had no effect (**Figure 4w**). Similar to βarr1, ghrelin-stimulated WT-βarr2 recruitment efficacy was markedly reduced by $GRK2^{K220R}$ (57% decrease) and moderately reduced by GRK2i (28% decrease), while ghrelin potency was unaffected (**Figure 4x-y**). For the L149P mutant, there was a trend for reduced constitutive βarr2 recruitment by $GRK2^{K220R}$, but this effect did not reach statistical significance relative to control. We did, however, identify a small, statistically significant increase in constitutive L149P-βarr2 recruitment by GRK2i when compared to $GRK2^{K220R}$ (**Figure 4z**). Similar to βarr1, $GRK2^{K220R}$ reduced ghrelin-stimulated L149P-βarr2 recruitment efficacy and GRK2i had no effect, while ghrelin potency was not affected in either condition (**Figure 4aa-bb**). Taken together, these results support that βarr1/2 recruitment to the L149P mutant requires GRK2/3-mediated receptor phosphorylation (*i.e.*, enzymatic activation), but it does not require Gβγ-dependent GRK2/3 activation; whereas, the WT-GHSR requires both of these processes for βarr1/2 recruitment.

To further test whether L149P recruits GRK2/3 in a Gβγ-independent manner, we performed BRET-based receptor-$GRK2^{YFP}$ recruitment assays [28] (**Figure 4cc**) in the presence or absence of GRK2i. Constitutive GRK2 recruitment was similar between WT and L149P under vehicle-treated conditions, and GRK2i did not affect constitutive GRK2 recruitment to either receptor (**Figure 4dd**). Consistent with our prediction, GRK2i pretreatment decreased WT-GRK2 recruitment efficacy, albeit mildly (10% decrease),

and did not affect L149P-GRK2 recruitment efficacy (**Figure 4ee-ff**). Ghrelin potency was not affected by GRK2i pretreatment for either receptor (see **Figure 4ee**). We suspect that the moderate effect of GRK2i on GRK2 recruitment to the WT receptor, at least relative to βarr1/2 (see **Figures 4q, 4r, 4x, and 4y**), was due to GRK2 over-expression in these experiments. Notably, the reduction GRK2 recruitment to the WT receptor following GRK2i pretreatment was statistically equivalent to L149P-GRK2 recruitment under vehicle-treated conditions (see **Figure 4ff**), supporting that reduced L149P-GRK2 recruitment at baseline is due to a lack of Gβγ-mediated GRK2 translocation. To further test this, we utilized a truncated GRK2 mutant, $GRK2^{\Delta V661\text{-}ct}$, which abrogates the Gβγ-GRK2 interaction by removing the far C-terminal Gβγ-binding (PH) domain of GRK2 [28]. Consistent with our GRK2i results (see **Figure 4dd**), there was no difference in constitutive (**Figure 4gg**) or ghrelin-stimulated (**Figure 4hh-ii**) $GRK2^{\Delta V661\text{-}ct}$ recruitment between the WT and L149P receptors (see **Figure 4ee-ff**).

To test if $G\alpha_{i/o}$ partial agonism (see **Figures 3s-z**) could explain Gβγ-independent βarr1/2 recruitment to L149P, we pretreated cells with $G\alpha_{i/o}$ inhibitor — pertussis toxin (PTX) [39] — then tested ghrelin-stimulated βarr1/2 recruitment. Ghrelin-induced βarr1 recruitment efficacy, but not potency, at the WT receptor was reduced moderately by PTX (**Supplementary Figure 1a**), while L149P-βarr1 recruitment was unaffected (**Supplementary Figures 1b-c**). For βarr2, ghrelin potency and efficacy/E_{max} were not affected by PTX at either receptor (**Supplementary Figure 1d-f**). Thus, $G\alpha_{i/o}$ signaling does not likely account for Gβγ-independent βarr1/2 (see **Figures 4aa-bb**) or GRK2 recruitment (see **Figures 3ee-ff, 4hh-ii**) to the L149P mutant.

Therefore, in contrast to the WT-GHSR, the L149P mutant recruits βarr1/2 and GRK2 in a G protein-independent manner — namely, independently of PKC, Gβγ-dependent GRK2/3 translocation, and $G\alpha_{i/o}$ — consistent with minimal G protein activation (see **Figure 3**). Nevertheless, the L149P mutant still requires enzymatic activation of GRK2/3 (*i.e.*, receptor phosphorylation) for βarr1/2 recruitment. For all descriptive data, C/R curve analyses, and statistics in **Figure 4**, see **Supplementary Table 5**.

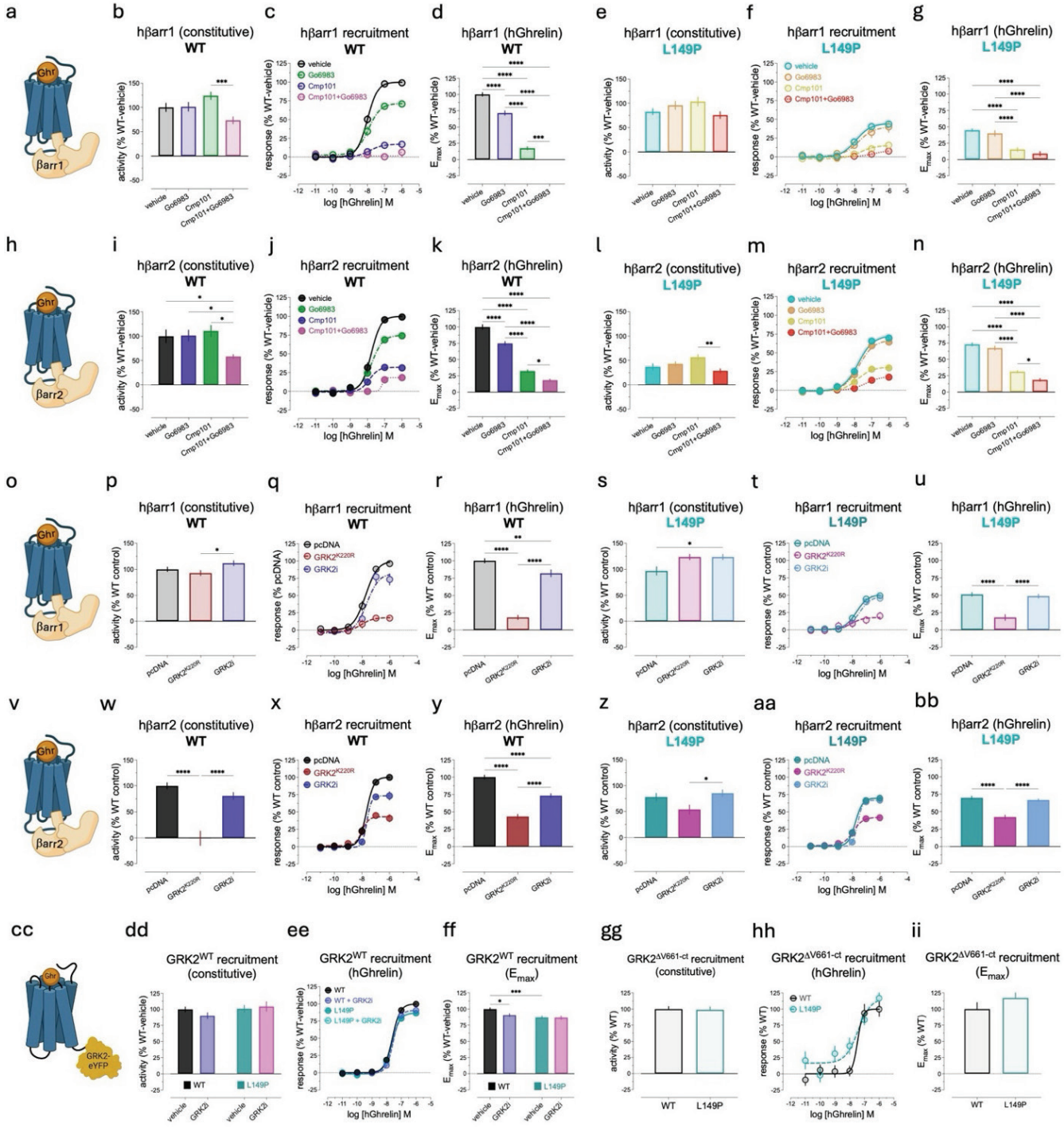

Figure 4. G protein-independent βarr1/2 and GRK2 recruitment to the L149P mutant. (a) hβarr1 recruitment to GHSR. **(b)** Constitutive, **(c)** hGhrelin C/R, and **(d)** hGhrelin E_{max} (derived from *Panel* c) of hβarr1 recruitment to WT following 30-minute pretreatment (RT) with vehicle (grey), Go6983 (light blue; 3μM), Cmp101 (light green; 10μM), or Go6983+Cmp101 (light purple). **(e)** Constitutive, **(f)** hGhrelin C/R, and **(g)** hGhrelin E_{max} (derived from *Panel f*) hβarr1 recruitment to L149P following pretreatment with vehicle (light teal), Go6983 (light orange), Cmp101 (light yellow), or Go6983+Cmp101 (light red). **(h)** hβarr2 recruitment to GHSR. **(i)** Constitutive, **(j)** hGhrelin C/R, and **(k)** hGhrelin E_{max} (derived from *Panel j*) of hβarr2 recruitment to WT following pretreatment with vehicle (black), Go6983 (dark blue), Cmp10 (dark green), or Go6983+Cmp101

(dark purple). **(l)** Constitutive, **(m)** hGhrelin C/R, and **(n)** hGhrelin E_{max} (derived from *Panel m*) hβarr2 recruitment to L149P following pretreatment with vehicle (dark teal), Go6983 (dark orange), Cmp101 (dark yellow), or Go6983+Cmp101 (dark red). **(o)** hβarr1 recruitment to GHSR. **(p)** Constitutive, **(q)** hGhrelin C/R, **(r)** hGhrelin E_{max} (derived from *Panel q*) of hβarr1 recruitment to WT following co-expression/pretreatment with pcDNA-vehicle (control; grey), $GRK2^{K220R}$-vehicle (light red), or pcDNA-GRK2i (100μM, 30-minutes, RT). **(s)** Constitutive, **(t)** hGhrelin C/R, **(u)** hGhrelin E_{max} (derived from *Panel t*) of hβarr1 recruitment to L149P in pcDNA-vehicle (light teal), $GRK2^{K220R}$-vehicle (light purple), or pcDNA-GRK2i (light blue). **(v)** hβarr2 recruitment to GHSR. **(w)** Constitutive, **(x)** hGhrelin C/R, **(y)** hGhrelin E_{max} (derived from *Panel x*) of hβarr2 recruitment to WT in pcDNA-vehicle (black), $GRK2^{K220R}$-vehicle (dark red), or pcDNA-GRK2i (dark blue). **(z)** Constitutive, **(aa)** hGhrelin C/R, **(bb)** hGhrelin E_{max} (derived from *Panel aa*) of hβarr2 recruitment to L149P in pcDNA-vehicle (dark teal), $GRK2^{K220R}$-vehicle (dark purple), or pcDNA-GRK2i (dark blue). All constitutive and E_{max} data were analyzed by one-way ANOVA. **(cc)** YFP-tagged WT-GRK2 ($GRK2^{WT}$) recruitment to GHSR. **(dd)** Constitutive, **(ee)** hGhrelin C/R, **(ff)** hGhrelin E_{max} (derived from *Panel ee*) of $GRK2^{WT}$ recruitment to WT-vehicle (black), WT-GRK2i (dark blue), L149P-vehicle (dark teal), and L149P-GRK2i (dark purple) following a 30-minute pretreatment (RT). Constitutive and E_{max} data were analyzed by two-way ANOVA followed by Tukey's post-hoc test. **(gg)** Constitutive, **(hh)** hGhrelin C/R, **(ii)** hGhrelin E_{max} (derived from *Panel hh*) of recruitment of $GRK2^{\Delta V661\text{-}ct}$ to WT (grey) or L149P (light teal). Constitutive and E_{max} data were analyzed by *t*-test. All data represent the pooled mean ± SEM from ≥3 independent experiments in duplicate or triplicate.

The L149P mutation switches the GRK recruitment profile of the GHSR.

βarr-biased ligands and receptors preferentially utilize GRK5/6 over GRK2/3 for βarr recruitment [26, 27]; thus, we next tested if the natural L149P mutation affects the receptor's GRK preference profile. To this end, we tested βarr1/2 recruitment to the WT and L149P receptors in HEK293/A cell lines lacking all GRKs (ΔGRK2/3/5/6), GRK2/3 (ΔGRK2/3), or GRK5/6 (ΔGRK5/6) [26].

For βarr1 (**Figure 5a**), WT constitutive activity was not affected by loss of any GRK's (**Figure 5b**). Conversely, ghrelin-stimulated βarr1 recruitment efficacy was abolished by ΔGRK2/3/5/6 and ΔGRK2/3, while ghrelin potency and efficacy were not affected by ΔGRK5/6 (**Figures 5c-d**). Thus, agonist-induced WT-βarr1 recruitment is entirely GRK2/3-dependent. Constitutive βarr1 recruitment to L149P was also not affected by loss of any GRK's (**Figure 5e**), and ghrelin-stimulated βarr1 recruitment efficacy was abolished in ΔGRK2/3/5/6 cells. While trends towards decreased L149P-βarr1 recruitment were observed for both ΔGRK2/3 and ΔGRK5/6 cells (**Figures 5f-g**), the effect did not reach statistical significance for ΔGRK5/6 and statistical comparisons were precluded for ΔGRK2/3 due to a poor curve fit.

For βarr2 (**Figure 5h**), constitutive recruitment to the WT receptor was not affected by knockout of any GRK's (**Figure 5i**); whereas, ghrelin-stimulated βarr2 recruitment efficacy was abolished in ΔGRK2/3/5/6, markedly reduced in ΔGRK2/3, and increased in ΔGRK5/6, further supporting that the WT-GHSR requires only the GRK2/3 subclass for βarr recruitment (**Figures 5j-k**). We speculate that the increase in WT-βarr2 recruitment might be due to the compensatory upregulation of GRK2/3 in the absence of GRK5/6, as observed in prior studies [26]. Ghrelin potency was not affected in any conditions

for the WT receptor (**Figure 5j**). For L149P, constitutive βarr2 recruitment was not affected by GRK knockout (**Figure 5l**); whereas, ghrelin-stimulated L149P–βarr2 recruitment efficacy was markedly reduced in ΔGRK2/3/5/6 and ΔGRK2/3 cells (**Figures 5m-n**), consistent with our pharmacological data (see **Figure 4m-n**). Notably, in contrast to the WT-GHSR, ghrelin-stimulated βarr2 recruitment efficacy to the L149P mutant was reduced in ΔGRK5/6 cells (**Figures 5m-n**). Like the WT receptor, ghrelin potency at L149P was not affected by knockout of any GRK's (**Figure 5m**).

To test GRK5/6 coupling directly, we next employed a BRET-based GRK5/6^{YFP} recruitment assay (**Figure 5o**). While constitutive (**Figure 5p**) and ghrelin-stimulated (**Figures 5q**) GRK5 coupling to the L149P mutant did not differ from the WT receptor, constitutive GRK6 coupling to L149P was markedly increased at baseline (**Figure 5r**) and remained elevated following ghrelin treatment (**Figures 5s**). Ghrelin stimulation did not increase GRK5/6 coupling at either receptor relative to their respective baselines (**Figures 5q, 5s**); thus, we expressed the data as non-normalized, absolute net BRET values.

Collectively, the results in **Figure 5** support that agonist-induced βarr recruitment to the L149P mutant is GRK2/3 and GRK5/6-dependent, while βarr recruitment to the WT-GHSR is exclusively GRK2/3-dependent. Furthermore, the L149P mutation markedly increases constitutive GRK6 coupling and maintains GRK6 coupling following agonist treatment; thus, selective GRK5/6-dependent βarr recruitment to the L149P mutant might be due to enhanced GRK6 'precoupling'. For all descriptive data, C/R analyses, and statistics in **Figure 5,** see **Supplementary Table 6**.

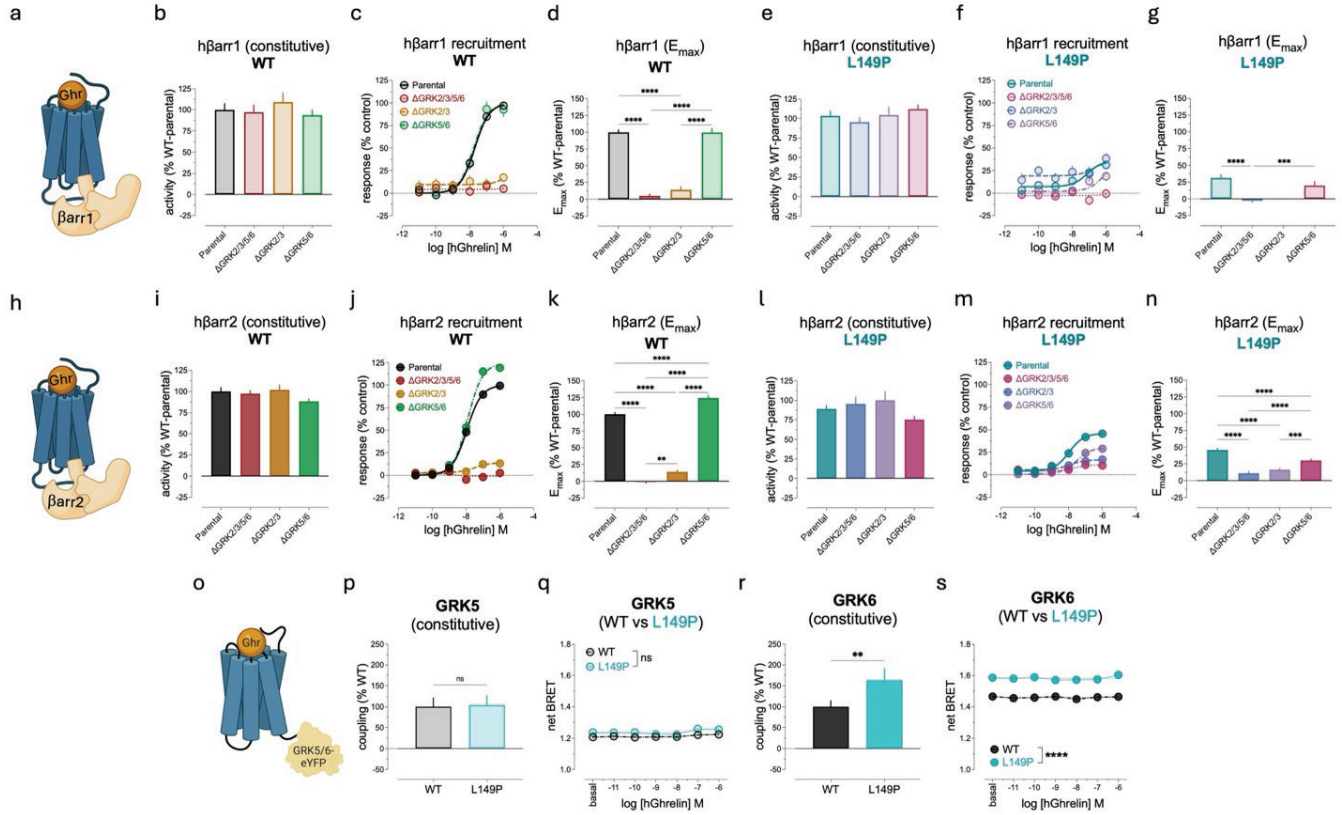

Figure 5. GRK subtype-specific βarr1/2 recruitment and GRK5/6 coupling to the L149P mutant. (a) hβarr1 recruitment to GHSR. **(b)** Constitutive, **(c)** hGhrelin-stimulated C/R, and **(d)** hGhrelin E_{max} (derived from *Panel c*) of hβarr1 recruitment to WT in parental (light grey), ΔGRK2/3/5/6 (light red), ΔGRK2/3 (light orange), and ΔGRK5/6 (light green). **(e)** Constitutive, **(f)** hGhrelin-stimulated C/R, and **(g)** hGhrelin E_{max} (derived from *Panel f*) of hβarr1 recruitment to L149P in parental (light teal), ΔGRK2/3/5/6 (light blue), ΔGRK2/3 (light purple), and ΔGRK5/6 (light maroon). **(h)** hβarr2 recruitment to GHSR. **(i)** Constitutive, **(j)** hGhrelin-stimulated C/R, and **(k)** hGhrelin E_{max} (derived from *Panel j*) of hβarr2 recruitment to WT in parental (dark grey), ΔGRK2/3/5/6 (dark red), ΔGRK2/3 (dark orange), and ΔGRK5/6 (dark green). **(l)** Constitutive, **(m)** hGhrelin-stimulated C/R, and **(n)** hGhrelin E_{max} (derived from *Panel m*) of hβarr2 recruitment to L149P in parental (dark teal), ΔGRK2/3/5/6 (dark blue), ΔGRK2/3 (dark purple), and ΔGRK5/6 (dark maroon). **(o)** GRK5/6^{YFP} coupling to GHSR. **(p)** Constitutive and **(q)** hGhrelin C/R-treated GRK5^{YFP} coupling, then **(r)** constitutive and **(s)** hGhrelin C/R-treated GRK6 ^{YFP} coupling over 30-minutes. *Panel p*, *r* were analyzed by Mann-Whitney nonparametric test; whereas, *Panels q, s* were analyzed by a mixed-model two-way ANOVA. All data represent the pooled mean ± SEM from 4 independent experiments in triplicate.

DISCUSSION

In this study, we identify and characterize an ultra-rare, coding variant in Leu149^{ICL2} [34.51] of the GHSR (L149P) — a prototypical rhodopsin-like GPCR. Our group has shown previously that the Leu149^{ICL2} residue, proximal to the highly conserved E/DRY motif, regulates transducer coupling [10] and receptor trafficking [14]. Herein, we expand upon this work by demonstrating that a natural missense mutation in Leu149^{ICL2} induces conformational states unfavorable to cholesterol-enriched PM microdomains (**Figure 1**) and G protein activation (**Figure 3**), despite robust βarr1/2 recruitment (**Figure 2)** and agonist-directed endosomal translocation (**Figures 1**). Furthermore, the L149P mutant switches the GRK selectivity profile of the GHSR from an exclusively GRK2/3-dependent, to a GRK2/3/5/6-dependent GPCR (**Figure 5**), which recruits βarr1/2 in a G protein-independent manner (**Figure 4**). Collectively, our results highlight how a single, naturally-occurring substitution in ICL2 can simultaneously influence receptor–lipid interactions, biased signaling, and intracellular trafficking (**Figure 6**).

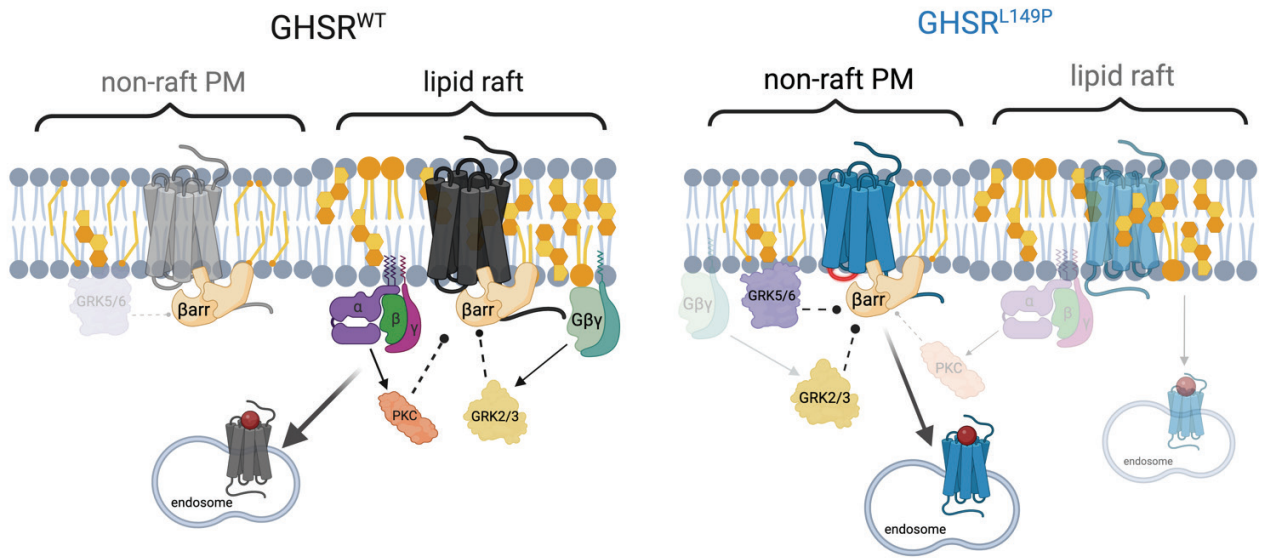

Figure 6. Simplified model of hypothesized L149P mechanisms. We hypothesize that the ultra-rare, natural L149P mutant (teal, *right*), destabilizes the α-helical conformation of ICL2, thereby (i) reducing clustering within cholesterol/sphingolipid-enriched lipid rafts and (ii) blocking G protein activation. Consequently, L149P preferentially partitions into more disordered, non-lipid raft PM microdomains (*e.g.*, unsaturated fatty acid-enriched) and exhibits poor agonist-directed endocytosis from lipid rafts. Under basal conditions, L149P expression is biased towards the PM over endosomes due to attenuated constitutive internalization/receptor cycling. However, upon agonist stimulation, L149P undergoes robust internalization and endosomal translocation via kinetics distinct from the WT-GHSR (black, *left*), suggesting that L149P may utilize different endocytic route(s). The L149P mutant readily recruits βarr in a cholesterol-dependent manner, while simultaneously inhibiting $G\alpha_q$ via decreased guanine nucleotide exchange. Accordingly, L149P does not activate PKC or Gβγ-dependent GRK2 translocation and recruits βarr in G protein-independent manner, despite weak $G\alpha_{i/o}$ partial agonism. In contrast to the WT-GHSR, βarr recruitment to L149P requires both GRK2/3 and GRK5/6, with the latter associated with increased L149P-GRK6 proximity. Thus, GRK6 precoupling to L149P might 'prime' the receptor for βarr coupling/recruitment, desensitization, and endocytosis.

First, we found that the natural L149P mutant enhances basal PM localization via decreased constitutive internalization (*i.e.*, receptor cycling) and secondarily, distrupts receptor distribution within its local lipid microenvironment; including, diminished clustering within cholesterol-enriched lipid rafts, (ii) preferential partitioning into non-raft PM microdomains, and (iii) markedly reduced lipid raft-mediated endocytosis. Despite the latter effect, ghrelin-stimulated L149P internalization and endosomal translocation was enhanced, suggesting that perturbation of ICL2 may redirect intracellular trafficking towards distinct route(s) relative to the WT-GHSR. Considering both the slower endosomal translocation kinetics and lipid raft enrichment of the WT-GHSR, it is possible that the WT receptor internalizes, at least in part, via a caveolin-dependent pathway, while the L149P mutant preferentially (or exclusively) utilizes βarr-dependent clathrin-mediated endocytosis. Additionally, these effects may reflect changes in receptor conformation and/or mobility near ICL2, as the orientation of GPCR transmembrane helices and loops (*e.g.*, inactive-to-active receptor states) determine their hydrophobic thickness, thereby impacting lipid interactions and partitioning [29]. The L149P mutant preferentially localized within non-raft PM microdomains, which are typically comprised of more disordered unsaturated lipids, suggesting that structural perturbations in ICL2 might favor insertion into more fluid membrane compartments. Accordingly, dietary changes in lipid composition (*e.g.*, high- *versus* low-fat diets) could alter the PM microenvironment and thereby, affect GHSR biased signaling/trafficking. The GHSR is highly sensitive to diet-derived nutrients and regulates energy balance via dynamic nutrient sensing [40]; thus, the effects of specific dietary lipids and dietary exposures on GHSR structure/function warrants further investigation.

Based on prior work demonstrating that ICL2 forms a short α-helix in active GPCR–transducer complexes (especially in Class A GPCRs [41, 42]), we speculate that "helix-breaking" mutations at $Leu149^{ICL2}$ — such as the previously characterized L149G [10, 14] or the natural L149P mutant described herein — reduces ICL2 α-helical stability and disrupts ICL2-E/DRY motif interactions critical to G protein activation. While glycine is more permissive than proline, both substitutions would likely decrease the stability ICL2 α-helices and thereby, explain why the $Leu149^{ICL2}$ mutants fail to initiate $G\alpha_q$ signaling.

Despite a lack of $G\alpha_q$ activation, the L149P mutant elicits high-affinity/low-efficacy mini-G_q coupling upon agonist stimulation, supporting prior work showing that $GPCR^{ICL2}$ mutations can prevent guanine nucleotide exchange without necessarily precluding G protein coupling [43]. Furthermore, our G protein selectivity results demonstrate that the L149P mutant exhibits partial agonism at $G\alpha_{i/o}$, while agonist-induced $G\alpha_q$ and $G\alpha_{13}$ signaling are abolished (see **Figure 3**). Importantly, membrane cholesterol is required for both constitutive and agonist-stimulated signaling at most G protein subtypes for the WT-GHSR, while any observable L149P-mediated G protein signaling is completely cholesterol-independent. Moreover, cholesterol depletion engenders changes to WT receptor-mediated G protein signaling that are directionally consistent with L149P at baseline (*e.g.*, MβCD-induced increase in constitutive WT-$G\alpha_{13}$ activity and attenuated agonist-induced $G\alpha_q$, $G\alpha_{13}$, and $G\alpha_{oA}$ activation). Notably, these results contrast with βarr, in which, cholesterol depletion disproportionately affects L149P relative to the WT-GHSR (see **Figure 2**). Given the differential distribution of $G\alpha_q$, $G\alpha_{13}$, and $G\alpha_{i/o}$ in caveolae [44], non-rafts [45], and lipid rafts [44], respectively, and that βarr may be recruited preferentially to non-raft microdomains [46], the signaling bias of L149P could be related, in part, to PM partitioning-dependent transducer proximity.

Despite markedly reduced G protein activation, the L149P mutant retains high intrinsic efficacy for βarr via mechanisms dependent on both its PM expression bias and membrane cholesterol (**Figure 2**). These results support that (i) ICL2 stability is a critical regulator of transducer coupling selectivity, (ii) G protein- and βarr-coupled GPCRs adopt distinct conformational states, and (iii) βarr recruitment is dependent on the receptor's subcellular distribution and microdomain partitioning (*i.e.*, location bias). Furthermore, L149P recruits βarr independently of both PKC and Gβγ-dependent GRK2/3 translocation (**Figure 4**), supporting that βarr recruitment can, in some cases, be dissociated from G protein signaling. Lastly, we found that the L149P mutant requires both the GRK2/3 and GRK5/6 subclasses for βarr recruitment, while the WT-GHSR requires only GRK2/3 (**Figure 5**). These results are consistent with other βarr-biased ligands [26] and intrinsically βarr-biased receptors [27], which preferentially utilize GRK5/6. Because GRK5/6 is membrane-anchored, the L149P mutant may disproportionately recruit this GRK subclass due to its PM expression bias and/or preferential partitioning into non-raft microdomains. Consistent with this notion, the L149P mutant exhibits elevated constitutive GRK6 pre-coupling and sustained GRK6 proximity following agonist stimulation (see **Figure 5**); thus, enhanced GRK6 pre-coupling could 'prime' L149P for βarr recruitment, desensitization (*i.e.*, G protein uncoupling), and internalization, as shown for other GRK2/3/5/6-dependent GPCRs (*e.g.*, β2-adrenergic receptor) [24]. More broadly, we propose that the $Leu149^{ICL2}$ locus acts as a conserved "bias hotspot" and therefore, provides a structural blueprint to rationally design βarr–biased ligands. Harnessing this "bias hotspot" pharmacologically with biased allosteric modulators, may offer a advantageous approach to achieve therapeutic efficacy while simultaneously reducing side effects [47].

While the clinical relevance of this ultra-rare *GHSR* SNP (rs1390872592) is currently unknown, our findings underscore how single amino acid mutations can confer dramatic changes to GPCR structure/function. In a physiological context, we speculate that the L149P mutation might reduce energy intake, body weight, and growth hormone secretion, as well as improve glucose control, by reducing GHSR-mediated $G\alpha_q$ signaling [9]. Because the Leu^{ICL2} site and neighboring residues (*e.g.*, GHSR-Pro148; [34.50]) are well-conserved across rhodopsin-like GPCRs, it is conceivable that other rare variants within this ICL2 locus could engender pathophysiological effects, especially when extrapolated across large, heterogenous populations.

METHODS

Cell Culture & Transfections

HEK293/T-17 cells (Cat no. CRL-11268) were purchased from the American Type Culture Collection (ATCC). HEK293/A parental (ThermoFisher; Waltham, MA) and their derivative CRISPR/Cas9-engineered GRK knockout (DGRK2/3/5/6, DGRK2/3, DGRK5/6) were described previously [26]. All cell lines were maintained in Dulbecco's Modified Eagle Medium (DMEM; Gibco, ThermoFisher; Cat no. 11995073) supplemented with 10% fetal bovine serum (FBS; Gibco, ThermoFisher; Cat no. 26140095) and antibiotic-antimycotic (Gibco, ThermoFisher; Cat no. 15240062) (complete DMEM). Cells were cultured in a humidified 5% CO_2 incubator at 37°C and grown on coated tissue culture plates. All cell lines were routinely split/passaged using trypsin/EDTA (Gibco, ThermoFisher; Cat no. 25200114) and never exceeded >30 passages.

For all transfections, cells were first seeded at a density of 6-7.5 x 10^5 cells/well in a 6-well plate. Then 16-24 hours later, cells were transfected using a standard calcium phosphate method. Transfection reagents — $CaCl_2$ (2.5M; Cat no. TBS5072) and HEPES-buffered saline (2xHBS, pH 7.05; Cat no. TBS5076) — were purchased from TriBioscience (Sunnyvale, CA). As described above, L149P was transfected at a 0.5:1 ratio relative to the WT-GHSR (typically 50ng:100ng, respectively) to adjust for total receptor expression (see **Figure 1c**), except when indicated otherwise (see **Figure 1b**). Dyn^{K44A}, ^{mVenus}hbarr1/2, and all GRK^{YFP} plasmids were transfected at a mass of 1mg, while TRUPATH sensors were all transfected at a mass of 100ng. Filler cDNA (pcDNA3.1+ or pcDNA5 for TRUPATH experiments) was used to bring the total transfection reaction mixture up to 2-3mg. Six-eight hours after transfection, the media was exchanged for complete DMEM, then incubated overnight prior to 96-well plate seeding (described below). All cell counting and transfection efficiency measurements were performed using a Countess 3 FL automated cell counter (ThermoFisher; Cat no. AMQAF2000).

Plasmids & Pharmacological Reagents

Plasmid cDNA synthesis and site-directed mutagenesis of the N-terminally hemagglutinin (3xHA)-tagged $hGHSR_{1a}^{WT}$, $hGHSR_{1a}^{L149P}$, $hGHSR_{1a}^{WT}$-RLuc8, $hGHSR_{1a}^{L149P}$-RLuc8 was performed by GenScript (Piscataway, NJ) and cloned into a pcDNA3.1+ vector backbone. For empty vector control conditions to measure constitutive activity (see **Figures 3-5**), pcDNA3.1+ was used. The rat dynamin-1 dominant negative, Dyn^{K44A}, was generated by the Caron Laboratory (Duke University; Durham, NC) and described previously [48]. The bBRET sensors mVenus-CAAX [49], (MyrPalm)-mVenus [6], and 2xFYVE-mVenus [50] have been described previously. The N-terminally mVenus-tagged human barr1 (hbarr1) and barr2 (hbarr2) plasmids were a gift from Dr. Lauren Slosky (University of Minnesota; Minneapolis, MN). All TRUPATH sensors were gifts from Dr. Bryan Roth (Addgene Kit #1000000163). The mini-G_q plasmid was a gift from Dr. Nevin Lambert (Augusta University; Augusta, GA). The dominant negative mutant, bovine GRK2-K220R, was a gift from Dr. Robert Lefkowitz (Addgene plasmid #35403). The $GRK2^{WT}$-YFP [28], $GRK2^{V661\text{-}ct}$-YFP [28], and GRK5/6-YFP [51] plasmids were described previously.

Human acyl-ghrelin (ghrelin), MK0677, Go6983, and Cmp101 were purchased from Tocris Bioscience (Bristol, UK). MbCD and GRK2i were purchased from MedChemExpress (Monmouth Junction, NJ). Pertussis toxin (PTX) was purchased from Cayman Chemical (Ann Arbor, MI).

On- and In-Cell ELISA Assays

ELISA assays were performed as previously described [6]. Briefly, transfected cells were seeded on poly-D-lysine-coated 96-well plates at a density of ~45,000 cells/well in phenol red-free opti-MEM (Gibco, ThermoFisher; Cat no. 11058021) supplemented with 2% FBS and antibiotic-antimycotic ('BRET media'). After overnight culture, BRET media was aspirated and serum-starved in opti-MEM (containing no FBS or antibiotic-antimycotic) for 2-4 hours prior to stimulation with vehicle (opti-MEM), ghrelin (1μM), or MK0677 (1μM) for 45-minutes at 37°C. Next, media was rapidly aspirated and fixed in 4% paraformaldehyde for 15-minutes at RT. Fixed cells were washed three times (~5-minutes/wash) in phosphate-buffered saline (PBS, pH 7.4; Gibco), then blocked for 1-hour in fish gelatin (Rockland Immunochemicals; Philadelphia, PA; Cat no. MB-067-0100). Cells were then probed with horseradish peroxidase (HRP)-conjugated anti-HA polyclonal antibody (Invitrogen, Cat no. PA1-29751) for 1-hour at RT (1:2,500). Next, cells were washed three times with PBS, then incubated with 1x SuperSignal™ West Pico PLUS Chemiluminescent Substrate (ThermoFisher; Cat no. 34577) for ~5-minutes prior to measuring luminescence in a TriStar3 multimodal plate reader (Berthold Technologies; Baden-Württemberg, Germany). For in-cell ELISA assays, blocking buffer, antibody buffer, and PBS wash buffer contained 0.2% triton-X-100 to permeabilize the cells. For on-cell ELISA assays, triton-X-100 was omitted in order to label only surface receptors.

bBRET and BRET1/2 Assays

All bBRET and BRET1/BRET2 assays were performed as previously described [6]. Briefly, transfected cells were seeded on poly-D-lysine-coated 96-well plates at a density of 40-45,000 cells/well in BRET media. After overnight culture, cells were serum-starved in Hank's Balance Salt Solution (HBSS; Gibco; Cat no. 14025134) supplemented with 20mM HEPES for 2-4 hours at 37°C. Then, cells were either pretreated with inhibitors for 30-minutes at RT or proceeded immediately to agonist treatment. Five-ten minutes prior to agonist treatment, cells were incubated with coelenterazine-H (NanoLight Technology; Pinetop, AZ; Cat no. 301) for BRET1 (mVenus/eYFP) or coelenterazine-400a (NanoLight; Cat no. 340) for BRET2 (GFP2) based on manufacturer instructions. All BRET measurements were taken on a TriStar3 plate reader set to 37°C for bBRET assays or RT (22-25°C) for all other assays using the recommended filter settings. All '*basal*' activity measurements represent the maximal absolute net BRET (acceptor/donor) of receptor-alone conditions (*i.e.*, non-normalized); whereas, all *'constitutive*' activity measurements represent the maximal difference between net BRET of receptor-alone minus the net BRET of pcDNA/EV-alone (*i.e.*, to derive D net BRET). All agonist-stimulated response data represent the maximal difference in the net BRET of agonist-stimulated conditions (at each ligand concentration) minus the net BRET of receptor-alone (*i.e.*, agonist D net BRET). To control for time-dependent effects, all D net BRET measurements (constitutive and agonist) were calculated/normalized relative to its respective control within the same column on a 96-well plate.

Statistics & Data Analysis

As indicated in the Figure Legends, all data are presented as the pooled mean±SEM derived from $\geq$3 independent experiments. For all biochemical experiments, 2-4 technical replicates were included. All data were plotted and analyzed in GraphPad Prism version 10 with a statistical significance threshold defined as $p<0.05$; ns, $p>0.05$, *, $p<0.05$; **, $p<0.01$; ***, $p<0.001$; ****, $p<0.0001$. All data represent the maximal responses over the full assay duration following vehicle or agonist treatment and are normalized to the WT top/E_{max} (100%) and bottom (0%), then fit by a three- or four-parameter non-linear regression determined statistically by an F-test.

REFERENCES

1. Hauser AS, Attwood MM, Rask-Andersen M, Schioth HB, Gloriam DE. Trends in GPCR drug discovery: new agents, targets and indications. Nat Rev Drug Discov. 2017;16(12):829-42.
2. Weis WI, Kobilka BK. The Molecular Basis of G Protein-Coupled Receptor Activation. Annu Rev Biochem. 2018;87:897-919.
3. Thompson MD, Percy ME, Cole DEC, Bichet DG, Hauser AS, Gorvin CM. G protein-coupled receptor (GPCR) gene variants and human genetic disease. Crit Rev Clin Lab Sci. 2024;61(5):317-46.
4. Eiger DS, Hicks C, Gardner J, Pham U, Rajagopal S. Location bias: A "Hidden Variable" in GPCR pharmacology. Bioessays. 2023;45(11):e2300123.
5. Kenakin T. Biased Receptor Signaling in Drug Discovery. Pharmacol Rev. 2019;71(2):267-315.
6. Gross JD, Kim DW, Zhou Y, Jansen D, Slosky LM, Clark NB, et al. Discovery of a functionally selective ghrelin receptor (GHSR(1a)) ligand for modulating brain dopamine. Proc Natl Acad Sci U S A. 2022;119(10):e2112397119.
7. Rajagopal S, Shenoy SK. GPCR desensitization: Acute and prolonged phases. Cell Signal. 2018;41:9-16.
8. Yanagi S, Sato T, Kangawa K, Nakazato M. The Homeostatic Force of Ghrelin. Cell Metab. 2018;27(4):786-804.
9. Gross JD, Zhou Y, Barak LS, Caron MG. Ghrelin receptor signaling in health and disease: a biased view. Trends Endocrinol Metab. 2023;34(2):106-18.
10. Evron T, Peterson SM, Urs NM, Bai Y, Rochelle LK, Caron MG, et al. G Protein and beta-arrestin signaling bias at the ghrelin receptor. J Biol Chem. 2014;289(48):33442-55.
11. Hedegaard MA, Holst B. The Complex Signaling Pathways of the Ghrelin Receptor. Endocrinology. 2020;161(4).
12. Mende F, Hundahl C, Plouffe B, Skov LJ, Sivertsen B, Madsen AN, et al. Translating biased signaling in the ghrelin receptor system into differential in vivo functions. Proc Natl Acad Sci U S A. 2018;115(43):E10255-E64.
13. Nagi K, Habib AM. Biased signaling: A viable strategy to drug ghrelin receptors for the treatment of obesity. Cell Signal. 2021;83:109976.
14. Toth K, Nagi K, Slosky LM, Rochelle L, Ray C, Kaur S, et al. Encoding the beta-Arrestin Trafficking Fate of Ghrelin Receptor GHSR1a: C-Tail-Independent Molecular Determinants in GPCRs. ACS Pharmacol Transl Sci. 2019;2(4):230-46.
15. Liu H, Sun D, Myasnikov A, Damian M, Baneres JL, Sun J, et al. Structural basis of human ghrelin receptor signaling by ghrelin and the synthetic agonist ibutamoren. Nat Commun. 2021;12(1):6410.
16. Qin J, Cai Y, Xu Z, Ming Q, Ji SY, Wu C, et al. Molecular mechanism of agonism and inverse agonism in ghrelin receptor. Nat Commun. 2022;13(1):300.

17. Shiimura Y, Horita S, Hamamoto A, Asada H, Hirata K, Tanaka M, et al. Structure of an antagonist-bound ghrelin receptor reveals possible ghrelin recognition mode. Nat Commun. 2020;11(1):4160.
18. Wang Y, Guo S, Zhuang Y, Yun Y, Xu P, He X, et al. Molecular recognition of an acyl-peptide hormone and activation of ghrelin receptor. Nat Commun. 2021;12(1):5064.
19. Gimpl G. Interaction of G protein coupled receptors and cholesterol. Chem Phys Lipids. 2016;199:61-73.
20. Casiraghi M, Damian M, Lescop E, Point E, Moncoq K, Morellet N, et al. Functional Modulation of a G Protein-Coupled Receptor Conformational Landscape in a Lipid Bilayer. J Am Chem Soc. 2016;138(35):11170-5.
21. Simons K, Toomre D. Lipid rafts and signal transduction. Nat Rev Mol Cell Biol. 2000;1(1):31-9.
22. Moreau CJ, Audic G, Lemel L, Garcia-Fernandez MD, Niescierowicz K. Interactions of cholesterol molecules with GPCRs in different states: A comparative analysis of GPCRs' structures. Biochim Biophys Acta Biomembr. 2023;1865(3):184100.
23. Kim DM, Lee JH, Pan Q, Han HW, Shen Z, Eshghjoo S, et al. Nutrient-sensing growth hormone secretagogue receptor in macrophage programming and meta-inflammation. Mol Metab. 2024;79:101852.
24. Drube J, Haider RS, Matthees ESF, Reichel M, Zeiner J, Fritzwanker S, et al. GPCR kinase knockout cells reveal the impact of individual GRKs on arrestin binding and GPCR regulation. Nat Commun. 2022;13(1):540.
25. Matthees ESF, Filor JC, Jaiswal N, Reichel M, Youssef N, D'Uonnolo G, et al. GRK specificity and Gbetagamma dependency determines the potential of a GPCR for arrestin-biased agonism. Commun Biol. 2024;7(1):802.
26. Kawakami K, Yanagawa M, Hiratsuka S, Yoshida M, Ono Y, Hiroshima M, et al. Heterotrimeric Gq proteins act as a switch for GRK5/6 selectivity underlying beta-arrestin transducer bias. Nat Commun. 2022;13(1):487.
27. Sarma P, Carino CMC, Seetharama D, Pandey S, Dwivedi-Agnihotri H, Rui X, et al. Molecular insights into intrinsic transducer-coupling bias in the CXCR4-CXCR7 system. Nat Commun. 2023;14(1):4808.
28. Pack TF, Orlen MI, Ray C, Peterson SM, Caron MG. The dopamine D2 receptor can directly recruit and activate GRK2 without G protein activation. J Biol Chem. 2018;293(16):6161-71.
29. Zhao LH, Lin J, Ji SY, Zhou XE, Mao C, Shen DD, et al. Structure insights into selective coupling of G protein subtypes by a class B G protein-coupled receptor. Nat Commun. 2022;13(1):6670.
30. Marion S, Oakley RH, Kim KM, Caron MG, Barak LS. A beta-arrestin binding determinant common to the second intracellular loops of rhodopsin family G protein-coupled receptors. J Biol Chem. 2006;281(5):2932-8.

31. Toth AD, Szalai B, Kovacs OT, Garger D, Prokop S, Soltesz-Katona E, et al. G protein-coupled receptor endocytosis generates spatiotemporal bias in beta-arrestin signaling. Sci Signal. 2024;17(842):eadi0934.
32. Olsen RHJ, DiBerto JF, English JG, Glaudin AM, Krumm BE, Slocum ST, et al. TRUPATH, an open-source biosensor platform for interrogating the GPCR transducerome. Nat Chem Biol. 2020;16(8):841-9.
33. Damian M, Marie J, Leyris JP, Fehrentz JA, Verdie P, Martinez J, et al. High constitutive activity is an intrinsic feature of ghrelin receptor protein: a study with a functional monomeric GHS-R1a receptor reconstituted in lipid discs. J Biol Chem. 2012;287(6):3630-41.
34. Wan Q, Okashah N, Inoue A, Nehme R, Carpenter B, Tate CG, et al. Mini G protein probes for active G protein-coupled receptors (GPCRs) in live cells. J Biol Chem. 2018;293(19):7466-73.
35. Du Y, Duc NM, Rasmussen SGF, Hilger D, Kubiak X, Wang L, et al. Assembly of a GPCR-G Protein Complex. Cell. 2019;177(5):1232-42 e11.
36. Franke RR, Konig B, Sakmar TP, Khorana HG, Hofmann KP. Rhodopsin mutants that bind but fail to activate transducin. Science. 1990;250(4977):123-5.
37. Rouault AAJ, Buscaglia P, Sebag JA. MRAP2 inhibits beta-arrestin recruitment to the ghrelin receptor by preventing GHSR1a phosphorylation. J Biol Chem. 2022;298(6):102057.
38. Koch WJ, Inglese J, Stone WC, Lefkowitz RJ. The binding site for the beta gamma subunits of heterotrimeric G proteins on the beta-adrenergic receptor kinase. J Biol Chem. 1993;268(11):8256-60.
39. Moss J, Vaughan M. ADP-ribosylation of guanyl nucleotide-binding regulatory proteins by bacterial toxins. Adv Enzymol Relat Areas Mol Biol. 1988;61:303-79.
40. Broglio F, Benso A, Gottero C, Prodam F, Grottoli S, Tassone F, et al. Effects of glucose, free fatty acids or arginine load on the GH-releasing activity of ghrelin in humans. Clin Endocrinol (Oxf). 2002;57(2):265-71.
41. Wingler LM, McMahon C, Staus DP, Lefkowitz RJ, Kruse AC. Distinctive Activation Mechanism for Angiotensin Receptor Revealed by a Synthetic Nanobody. Cell. 2019;176(3):479-90 e12.
42. Liu X, Masoudi A, Kahsai AW, Huang LY, Pani B, Staus DP, et al. Mechanism of beta(2)AR regulation by an intracellular positive allosteric modulator. Science. 2019;364(6447):1283-7.
43. Powers AS, Khan A, Paggi JM, Latorraca NR, Souza S, Salvo JD, et al. A non-canonical mechanism of GPCR activation. bioRxiv. 2023.
44. Oh P, Schnitzer JE. Segregation of heterotrimeric G proteins in cell surface microdomains. G(q) binds caveolin to concentrate in caveolae, whereas G(i) and G(s) target lipid rafts by default. Mol Biol Cell. 2001;12(3):685-98.
45. Waheed AA, Jones TL. Hsp90 interactions and acylation target the G protein Galpha 12 but not Galpha 13 to lipid rafts. J Biol Chem. 2002;277(36):32409-12.

46. Zheng H, Chu J, Qiu Y, Loh HH, Law PY. Agonist-selective signaling is determined by the receptor location within the membrane domains. Proc Natl Acad Sci U S A. 2008;105(27):9421-6.
47. Slosky LM, Caron MG, Barak LS. Biased Allosteric Modulators: New Frontiers in GPCR Drug Discovery. Trends Pharmacol Sci. 2021;42(4):283-99.
48. Barak LS, Oakley RH, Laporte SA, Caron MG. Constitutive arrestin-mediated desensitization of a human vasopressin receptor mutant associated with nephrogenic diabetes insipidus. Proc Natl Acad Sci U S A. 2001;98(1):93-8.
49. Zheng K, Smith JS, Eiger DS, Warman A, Choi I, Honeycutt CC, et al. Biased agonists of the chemokine receptor CXCR3 differentially signal through Galpha(i):beta-arrestin complexes. Sci Signal. 2022;15(726):eabg5203.
50. Snyder JC, Rochelle LK, Ray C, Pack TF, Bock CB, Lubkov V, et al. Inhibiting clathrin-mediated endocytosis of the leucine-rich G protein-coupled receptor-5 diminishes cell fitness. J Biol Chem. 2017;292(17):7208-22.
51. Smith JS, Alagesan P, Desai NK, Pack TF, Wu JH, Inoue A, et al. C-X-C Motif Chemokine Receptor 3 Splice Variants Differentially Activate Beta-Arrestins to Regulate Downstream Signaling Pathways. Mol Pharmacol. 2017;92(2):136-50.

FUNDING

This work was supported by J.D.G. start-up funds from The Pennsylvania State University College of Health and Human Development and Huck Institute of the Life Sciences.

AUTHOR CONTRIBUTIONS

Conceptualization: A.T., L.S.B. and J.D.G.; *Methodology*: A.I. and J.D.G.; *Investigation/Performed Experiments*: E.M.B., L.K., J.A.S., and J.D.G.; *Data/Statistical Analysis*: A.T. and J.D.G.; *Writing*: A.T. and J.D.G.; *Review/Editing*: E.M.B., A.T., L.K., A.I., L.S.B., and J.D.G.

COMPETING INTERESTS

We have no competing interests to report for this manuscript.

DATA & MATERIALS

All data required to evaluate the results and conclusions in this manuscript are presented in the main and supplementary figures and tables. All materials generated for, or used in, this manuscript are described in the *Methods*.

SUPPLEMENTARY FIGURES

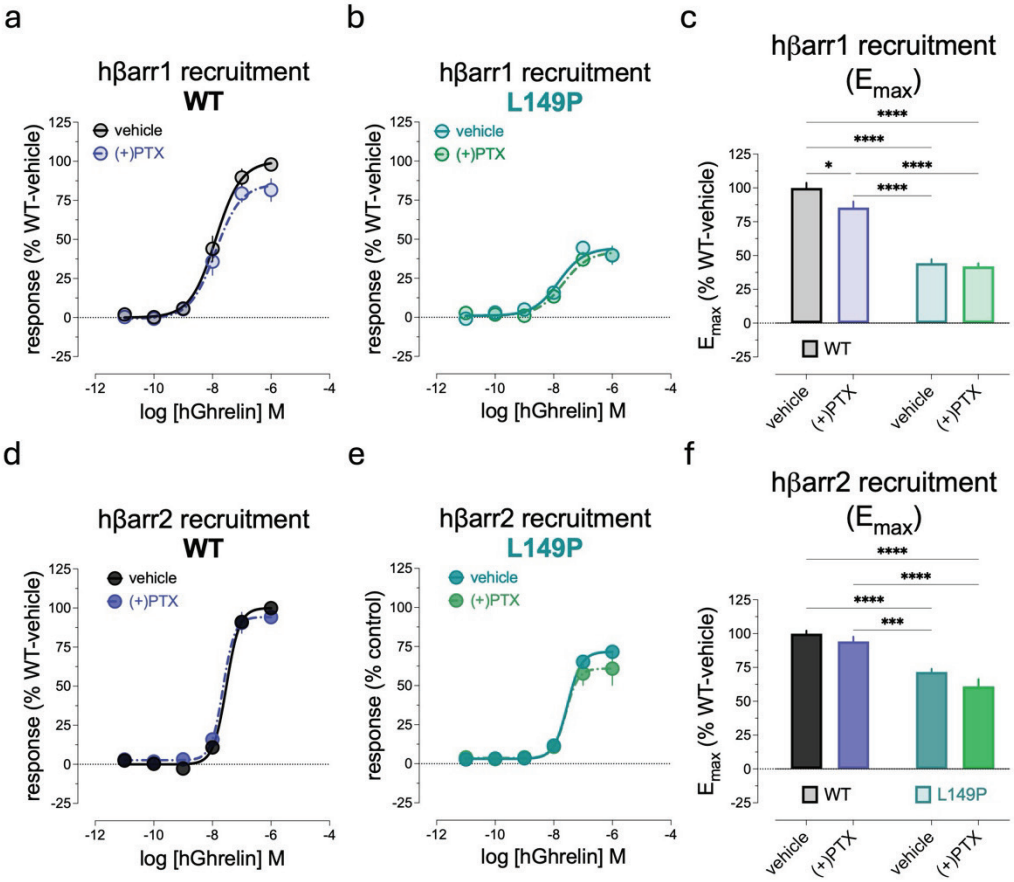

Supplementary Figure 1. Agonist-stimulated hβarr1/2 recruitment to L149P is $G\alpha_{i/o}$-independent. (a) hGhrelin (C/R)-induced hβarr1 recruitment to WT following vehicle (grey) or overnight PTX (200ng/mL; light blue) pretreatment. **(b)** hGhrelin (C/R)-induced hβarr1 recruitment to L149P following vehicle (light teal) or PTX pretreatment. **(c)** hGhrelin E_{max} (derived from *Panels a-b*) of hβarr1 recruitment to WT (*left*) and L149P (*right*) ± PTX. **(d)** hGhrelin (C/R)-induced hβarr2 recruitment to WT following vehicle (black) or overnight PTX (200ng/mL; dark blue) pretreatment. **(e)** hGhrelin (C/R)-induced hβarr2 recruitment to L149P following vehicle (dark teal) or PTX pretreatment. **(f)** hGhrelin E_{max} (derived from *Panels d-e*) of hβarr2 recruitment to WT (*left*) and L149P (*right*) ± PTX. All data represent the pooled mean ± SEM from 3 independent experiments run in duplicate.